CHALMERS
UNIVERSITY OF TECHNOLOGY

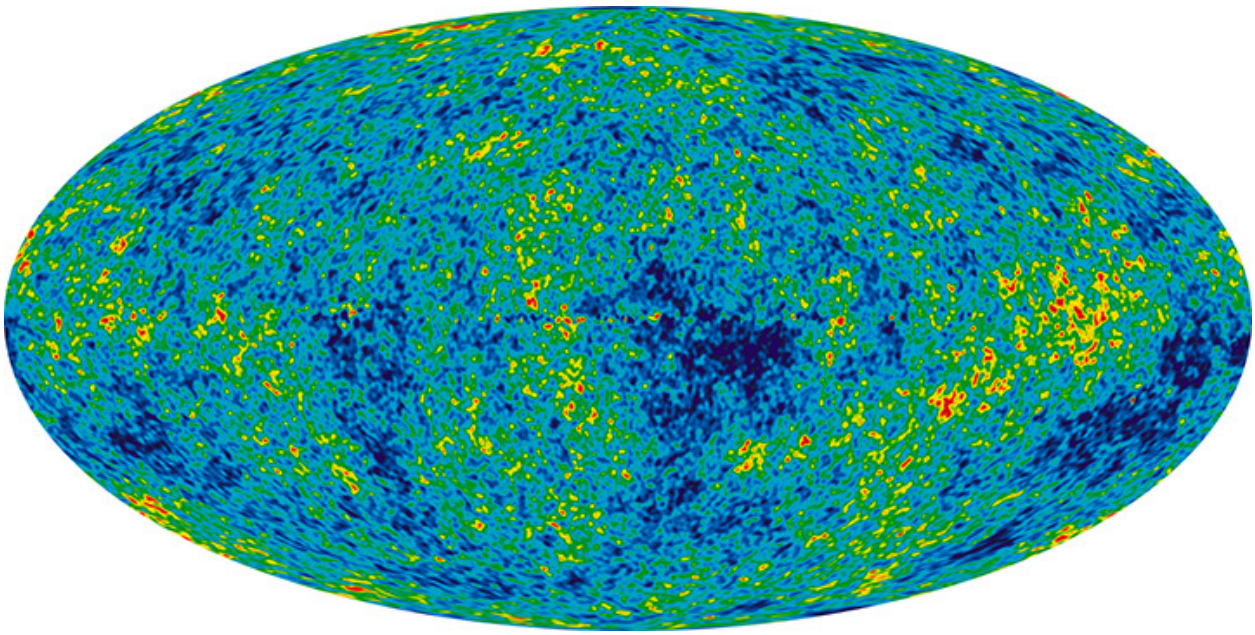

Strongly coupled massive flavor fields on de Sitter spacetime

Holographically computing the 1-point function dual to the massive D3/D7 scalar slipping mode in dS_4-sliced AdS_5

Master's thesis in Physics and Astronomy

EMIL LEEB-LUNDBERG

Department of Theoretical Physics
CHALMERS UNIVERSITY OF TECHNOLOGY
Gothenburg, Sweden 2017

Master's thesis 2017:NN

Strongly coupled massive flavor fields on de Sitter spacetime

Holographically computing the 1-point function dual to the massive D3/D7 scalar slipping mode in dS_4-sliced AdS_5

EMIL LEEB-LUNDBERG

Department of Theoretical Physics
Chalmers University of Technology
Gothenburg, Sweden 2017

Strongly coupled massive flavor fields on de Sitter spacetime.
Holographically computing the 1-point function dual to the massive D3/D7 scalar slipping mode in dS_4-sliced AdS_5.
EMIL LEEB-LUNDBERG

Supervisor: Professor Andreas Karch, University of Washington
Examiner: Professor Bengt E. W. Nilsson, Chalmers University of Technology

Master's Thesis 2017:NN
Department of Theoretical Physics
Chalmers University of Technology
SE-412 96 Gothenburg
Telephone +46 31 772 1000

Nine year microwave background sky image created using WMAP,
taken from http://map.gsfc.nasa.gov/media.

Typeset in LaTeX
Gothenburg, Sweden 2017

Acknowledgements

I want to thank my dear friends Carl, David, and Erik for all the wonderful times we had together at Chalmers. I want to thank Jonas, Fynn, Konstantin and Robin for a great time in Seattle. I want to thank Ufuk for his advice when I was choosing my Bachelor's program, "If you can't do math you're stupid," and Niclas for his advice when I was choosing a Master's program, "If you can't do QFT you're stupid." At some point or another I've been inspired by all of you. I'd especially like to thank my parents for always supporting and believing in me... not that they didn't expect it.

I'm very grateful for the teachers at the department of physics at Chalmers. I'd like to thank Professor Ulf Gran for his advice, and Professor Bengt Nilsson for helping with the administrative aspects of this thesis. I am also very appreciative of the hospitality of the theory group at the University of Washington. Finally, I'd like to sincerely thank Professor Andreas Karch, for all his enthusiasm, insight, and kindness.

Emil Hakan Leeb-Lundberg, Gothenburg, June 2017

Contents

1

Introduction

Attempting to understand the nature of cosmological inflation has united some of the most exciting fields of both experimental and theoretical physics. The investigation utilizes the oldest light in the universe, the cosmic microwave background (CMB) radiation, as a tool to probe the physics of how the universe is believed to have inflated to at least 10^{26} times its original size, some 10^{-36} seconds after the Big Bang singularity. Although the CMB appears to be homogeneous on a larger scale, closer inspection has shown it to have tiny inhomogeneities, known as temperature anisotropies, that are presumed to be the result of quantum fluctuations during inflation. This implies that there is a picture across the whole sky, on the scale of the universe, that can be traced back to the quantum scale fluctuations in the very early universe.

In attempting to explain these observations, an inflationary paradigm has been constructed, and for the single-field slow-roll model, inflation is sourced by the scalar inflaton field on de Sitter (dS) spacetime. To account for temperature anisotropies measured in the CMB, models suggest that the universe inflated unevenly due to scalar perturbations of the dS metric induced by quantum fluctuations of the inflaton field. More specifically, the temperature anisotropies are traced back to correlation functions of the scalar perturbations of the metric, and subsequently, correlation functions of the inflaton fluctuations. Observational evidence suggests that the scalar perturbations of the metric are nearly Gaussian and scale invariant [1], which is interpreted as the inflaton being scale invariant and weakly coupled, as the path integral measure of a free theory is Gaussian. In the case of single-field slow-roll inflation, the growth of the metric is facilitated by the inflaton field slowly rolling down a nearly flat potential, such that the self-interaction of the inflaton is suppressed during the period of inflation, resulting in a weakly coupled theory, with nearly Gaussian 2-point correlation functions [2]. Although observations suggest nearly Gaussian and scale invariant perturbations of the metric, measuring non-Gaussianity, which corresponds to measuring the interaction of the inflaton field [3], would significantly advance our understanding of inflationary dynamics [1]. A non-Gaussian measurement would, in terms of correlation functions, be the measurement of a 3-point correlation function of the scalar perturbation of the metric, and observing large non-Gaussianity would suggest a strongly interacting inflaton. Issues such as these call for the further investigation of correlation functions of quantum field theories at various coupling strengths on de Sitter spacetime.

Holography provides tools to map gravitational theories to field theories, and, by

formulating the gravitational theory in different ways, it is possible to vary the field theory it maps to. Moreover, field theory correlation functions to be computed holographically by relating them to gravitational computations. Motivated by current issues in inflation, this thesis aims to use holography to study the correlation functions of a strongly coupled field theory on dS_4. This is accomplished using a configuration known as the D3/D7 scalar slipping mode [4], which will now be considered. By first embedding a probe D7-brane on the gravitational side of the $\mathrm{AdS}_5/\mathrm{CFT}_4$ correspondence [5], where AdS_5 is foliated by slices of dS_4, it is possible to add massive flavor degrees of freedom to a strongly coupled field theory on dS_4, breaking conformal invariance. In this case, there is a scalar field on the worldvolume of the D7-brane that corresponds to a massive $\mathcal{N} = 2$ hypermultiplet of flavor fields in the field theory. Then, minimizing the worldvolume of the D7-brane corresponds to computing the 1-point function of the hypermultiplet on dS_4. Holographically computing the 1-point function of a strongly coupled hypermultiplet of flavor fields on dS_4, dual to the probe D7-brane slipping mode, is the objective of this thesis.

Previous studies have been conducted using holography as a tool to study strongly coupled quantum field theories on dS_4. In [6], the stress-energy tensor of a strongly coupled conformal field theory was studied on the de Sitter static patch using holography. In [7], the holographic dual of a massive probe D7-flavor brane embedded in dS_4-sliced AdS_5 was studied numerically. In this case, the dilaton, axion and self-dual five form field were retained at the level of the D7-brane action. Similar D3/D7 configurations have been used to study separate topics, such as [8], where a probe D7-brane was used to numerically compute the mass and condensate of a field theory on AdS_4.

This thesis is organized as follows. Chapter 2 sets the scene for holographically computing strongly coupled field theories on de Sitter space. Section 2.1 introduces the cosmic microwave background, inflation, and the inflaton field. Section 2.2 discusses some concepts in quantum field theory, including coupling, divergences, renormalization, beta functions, the large N_c limit, symmetries, and $\mathcal{N} = 4$ Super Yang-Mills theory. Section 2.3 introduces string theory, type IIB superstring theory, and supergravity. Section 2.4 introduces D-branes and their role in string theory. Section 2.5 introduces the AdS/CFT correspondence. Section 2.6 covers the relevant coordinate systems for hyperspheres, anti-de Sitter, de Sitter, and how foliation is performed on anti-de Sitter spacetime. Section 2.7 discusses how to add flavor to AdS/CFT, with an emphasis on the D7-brane slipping mode. In section 3.1 a massive probe D7-brane is embedded in $AdS_5 \times S^5$, where AdS_5 is foliated Minkowski spacetime, and the action and boundary asymptotics of the scalar slipping mode are computed. Section 3.2 discusses holographic renormalization and boundary conditions for the slipping mode. In section 3.3 the flat-slicing slipping mode equation of motion (EOM) is solved numerically and compared to the known supersymmetric background solution to ensure the numerical solver is functioning correctly. In section 4.1.1 a probe D7-brane is embedded in dS_4-sliced AdS_5. In section 4.1.2, asymptotic solutions at the boundary are discussed. In section 4.1.3 the asymptotic solution is acquired for dS_4-sliced AdS_5 by performing a near-boundary expansion.

In section 4.2 the slipping mode EOM is solved numerically in this background for both small and large masses. In section 4.3 the correction to the mass is computed by performing a large mass expansion. In section 4.4 coordinates are switched in order to compute the smallest mass solutions located behind the de Sitter horizon. In section 4.4.1 the embedding is described in the new coordinates, where there is the possibility of using new boundary conditions. In section 4.4.2 the analytical form of the smallest mass solutions is acquired using the new boundary conditions. In section 4.5, the slipping mode EOM is solved behind the horizon using two separate boundary conditions for both small and large masses.

2

Background

2.1 Inflation

The inflationary paradigm is the collection of models in cosmology that describe cosmic inflation, which is a period in the early universe in which space expanded exponentially, approximately 10^{-34} seconds after the big bang singularity. A cosmic observable that is believed to probe this process is the cosmic microwave background (CMB) radiation, which is the thermal black-body radiation of temperature $T \approx 2.7K$ leftover from the recombination epoch, some 300,000 years after the big bang. This radiation is present across the whole sky, and nearly homogeneous, except for small fluctuations on the order of 10^{-5}, known as temperature anisotropies [9]. Observations by the WMAP satellite have confirmed these anisotropies to great accuracy [10]. Inflationary models suggest these temperature anisotropies may be traced back to quantum fluctuations during the very early universe.

Cosmological inflation is described by a flat Friedmann-Robertson-Walker universe with accelerating scale factor $\ddot{a}(t) > 0$, equivalent to a shrinking co-moving horizon $\frac{d}{dt}(aH)^{-1} < 0$, where $H = \partial_t \ln a$ is the Hubble parameter. In this context, the Friedmann equation reads

$$H^2 = \left(\frac{\dot{a}}{a}\right)^2 = \frac{\rho}{3M_P^2}, \tag{2.1}$$

where M_p is the Planck mass, and ρ is the field density. Inflation must be sustained long enough for the scale factor to grow by a factor of e^{60}, during which H is approximately constant, yielding an exponential scale factor $a(t) \approx e^{Ht}$ [9]. Consequently, the geometry during inflation is approximately de Sitter (dS), which in the spatially flat gauge reads

$$ds^2 = -dt^2 + a^2(t)\delta_{ij}dx^i dx^j, \tag{2.2}$$

where $i, j = 1, 2, 3$. For single-field slow-roll inflation, the exponential growth is sourced by a scalar inflaton field ϕ, that is minimally coupled to gravity, with a potential that is almost flat. The model combines the Einstein-Hilbert action with that of a scalar field $S = S_{EH} + S_\phi$, given by

$$S = \int dx^4 \sqrt{-g}\left(\frac{1}{2}R - \frac{1}{2}g^{\mu\nu}\partial_\mu\phi\partial_\nu\phi - V(\phi)\right). \tag{2.3}$$

where the metric is given by (2.2), and $V(\phi)$ is the inflaton potential. Extremizing the inflaton action yields the equation of motion

$$\ddot{\phi} + 3H\dot{\phi} + V'(\phi) = 0, \tag{2.4}$$

where $V' = \partial_\phi V$. Then, by combining the energy-momentum tensor $T_{\mu\nu} = -\frac{2}{\sqrt{-g}}\frac{\delta S_\phi}{\delta g^{\mu\nu}}$ with the assumption of a perfect fluid $T^{\mu\nu} = \text{diag}\{\rho, -p, -p, -p\}$, the field pressure and density can be expressed as

$$\rho = \frac{1}{2}\dot{\phi}^2 + V(\phi), \qquad p = \frac{1}{2}\dot{\phi}^2 - V(\phi). \tag{2.5}$$

Combining the scalar field density (2.5) with the Friedmann equation (2.1), then gives the constraint

$$3M_P^2 H^2 = \frac{1}{2}\partial_t\phi + V(\phi). \tag{2.6}$$

The slow-roll regime is characterized by $\ddot{\phi} \ll H\dot{\phi} \sim V'(\phi)$ for equation (2.4), and $\dot{\phi}^2 \ll M_P^2 H^2 \sim V(\phi)$ for equation (2.1). This ensures that the field rolls slowly due to the flat potential $V(\phi)$. This regime is commonly described by the slow-roll parameters

$$\epsilon = \frac{\dot{\phi}^2}{2M_P^2 H^2} = -\frac{\dot{H}}{H^2}, \qquad \eta = -\frac{\ddot{\phi}}{H\dot{\phi}} = \frac{\ddot{H}}{H^3} \tag{2.7}$$

where the spacetime inflates as long as $\epsilon, \eta \ll 1$.

On a quantum scale, the inflaton field fluctuates $\phi(t, x^i) = \phi(t) + \delta\phi(t, x^i)$, where $\phi(t)$ is a spatially homogeneous solution, and $\delta\phi(t, x^i)$ is the fluctuation. The fluctuations $\delta\phi(t, x^i)$ induce scalar perturbations $\zeta(t, x^i)$ of the metric (2.2) [11], which can be seen by switching to the co-moving gauge

$$ds^2 = -dt^2 + a^2(t)e^{2\zeta(t,x^i)}\delta_{ij}dx^i dx^j. \tag{2.8}$$

Using a time reparameterization, it is possible to relate $\zeta(t, x^i) \sim H\delta t(x^i)$ [2], which implies that inflation occurred for different periods of time at different points in space due to the time delay $\delta t(x^i)$. It is this inhomogeneous growth of the universe during inflation that is believed to source the temperature anisotropies seen in the CMB [1]. The temperature anisotropies can be related to the inflaton fluctuations $\delta\phi$ by first Fourier transforming to momentum space $\delta\phi_k(t) = \int d^3x e^{ix_j k^j}\delta\phi(t, x^j)$, then considering how the modes $\delta\phi_k$ are affected by the shrinking co-moving horizon $(aH)^{-1}$. At the beginning of inflation, the modes $\delta\phi_k$ are inside the co-moving horizon $(aH)^{-1} \gg k^{-1}$. As inflation happens, the co-moving horizon shrinks, and a point comes at which the modes exit the co-moving horizon $(aH)^{-1} = k^{-1}$ and stop oscillating. By the end of inflation, the modes are frozen well outside the co-moving horizon $(aH)^{-1} \ll k^{-1}$. After inflation, the co-moving horizon grows again, allowing the frozen modes to re-enter the horizon and continue oscillating [1]. In addition to the preservation of $\delta\phi_k$ outside the horizon, the scalar perturbations of the metric, ζ_k, are also preserved. In terms of correlation functions evaluated at horizon exit, the scalar perturbations and modes are related by

$$\langle\zeta_k, \zeta_{k'}\rangle \sim \frac{H^2}{\dot{\phi}^2}\langle\delta\phi_k, \delta\phi_{k'}\rangle, \tag{2.9}$$

where for slow-roll inflation $\langle \delta\phi_{\vec{k}}, \delta\phi_{\vec{k}'} \rangle \sim \frac{H^2}{k^3}\delta(\vec{k} - \vec{k}')$ [2]. From (2.9), it is possible to compute the power spectrum $P_\zeta(k)$ which reads

$$\langle \zeta_{\vec{k}}, \zeta_{\vec{k}'} \rangle \sim P_\zeta(k)\delta(\vec{k} - \vec{k}'). \tag{2.10}$$

By combining the power spectra frozen at the horizon exit, with transfer functions associated with cosmological evolution after horizon re-entry, it is possible to account for how fluctuations in the inflaton field $\delta\phi$ source the temperature anisotropies ΔT seen in the CMB [1].

Measuring non-Gaussianity at the level of the CMB temperature anisotropies measures the degree of interaction at the level of the inflaton field [3]. Any dependence of the potential on the inflaton, results in interactions. For slow-roll inflation, the derivatives of the potential (the slow-roll parameters) are kept small in order to keep the potential flat, suppress interactions, and facilitate inflation. In this sense, the slow-roll parameters describe how weakly coupled the theory is. There has been no experimentally observed non-Gaussianity in the CMB. Consequently, the inflaton is assumed to be weakly coupled, and the standard inflationary paradigm slow-rolls at a nearly flat potential.

2.2 Field theory

One of the most attractive features of the AdS/CFT correspondence is its ability to relate weakly coupled string theories to strongly coupled quantum field theories (QFTs). In general, computing observables in strongly coupled QFTs is difficult due to the lack of a small coupling constant in which to perturbatively expand. For AdS_5/CFT_4, the a string theory is mapped to the strongly coupled $\mathcal{N} = 4$ super Yang-Mills (SYM) gauge theory. In order to sketch the field theory side of AdS/CFT, this section considers some of the concepts underlying $\mathcal{N} = 4$ SYM. This proceeds by first addressing perturbative expansion, divergences, and gauge theories, then discussing the role of symmetry in QFTs.

The method of perturbatively expanding weakly coupled field theories carries with it intrinsic divergences. The divergences occur in two types: UV divergences, which correspond to infinities in the expansion at high energies and small distances, and IR divergences, which correspond to infinities at low energies and large distances. To deal with such divergences, one typically employs regularization through one of two methods: dimensional regularization or via a cutoff. Thereafter, the theory is renormalized, which involves introducing counter terms to cancel infinities present in the bare terms. The result is renormalized terms, which are physical and dependent on some scale introduced in the regularization procedure. The renormalized terms, being dependent on a scale (e.g. energy scale), will vary, or "run", when the scale is changed. These scale transformations build a group known as the Renormalization Group (RG), and the relationship between the bare terms and the renormalized terms is represented by the RG equation. The running of the coupling constant and other parameters present in the original Lagrangian (e.g. field, mass) can be

determined through this equation. More specifically, the RG equation contains the β function, which describes how the coupling constant runs with scale, and the so-called anomalous dimensions, which describe how other parameters (e.g. mass, field) run with the scale [12].

When the β function vanishes, the coupling constant no longer runs with the mass scale, i.e. the coupling is scale invariant. The value of the coupling at which the β function vanishes is called a fixed point. A special case is the fixed point for which the coupling goes to zero while the cutoff goes to infinity; this is known as asymptotic freedom. For an asymptotically free theory, the coupling is strong at low energies, and weak at high energies.

Quantum field theories can also be afflicted with anomalies, which is when symmetries present in the classical theory are not preserved during the process of quantization. One example of an anomalous theory is massless ϕ^4 theory in $d = 4$, which is renormalizable, and has a dimensionless coupling constant. Quantization, however, results in divergences, which, when handled through regularization then renormalization, introduce a renormalization scale that breaks scale invariance.

Gauge transformations in field theories refer to transformations between redundant degrees of freedom that describe the same physical state. These transformations build a Lie group. If the generators commute, the theory is called Abelian, and non-Abelian if they do not commute. Quantum electrodynamics is an Abelian gauge theory with a U(1) symmetry. On the other hand, quantum chromodynamics is an example of a non-Abelian gauge theory with an SU(3) symmetry.

Non-Abelian gauge theories have many interesting characteristics: they exhibit asymptotic freedom, as the coupling strength decreases with increasing energy, and color confinement, as the quarks are bound by gluons, and thus confined to hadrons. Moreover, a relationship between non-Abelian gauge theories and string theory has been discovered. For the non-Abelian SU(N_c) Yang-Mills theory the β function is

$$\beta(g_{YM}) = \mu \frac{dg_{YM}}{d\mu} = -\frac{11}{3} N_c \frac{g_{YM}^3}{16\pi^2} + \mathcal{O}(g_{YM}^5), \tag{2.11}$$

where N_c is the number of colors, and g_{YM} is the coupling constant. Due to asymptotic freedom, SU(N_c) Yang-Mills theory is strongly coupled at low energies, making perturbative expansions unfeasible. This can be circumvented, however, by taking the limit in the dimensionless parameter $N_c \to \infty$, while letting $g_{YM} \to 0$, such that $\lambda \equiv g_{YM}^2 N_c$ is constant [13]. Here, λ is known as the 't Hooft coupling. What results from this is that the gauge theory simplifies in the Large N_c limit, and perturbative expansions in $1/N_c$ in this regime correspond to the perturbative expansions of strings, with string couplings proportional to $1/N_c$.

Symmetry and groups play a central role in QFTs, and discussion begins by reminding the reader of the Lorentz group. The Lorentz transformations (spatial boosts and rotations of $R^{1,3}$) build the Lorentz group SO(1, 3), whose generators $J_{\mu\nu}$ obey

	Transformation	Operator
Translation	$x^\mu \to x^\mu + a$	P_μ
Lorentz	$x^\mu \to \Lambda^\mu_\nu x^\nu$	$J_{\mu\nu}$
Dilatation	$x^\mu \to \lambda x^\mu$	D
Special Conformal	$x^\mu \to \frac{x^\mu + b^\mu x^2}{1+2bx+b^2x^2}$	K_μ
Inversion	$x^\mu \to \frac{x^\mu}{x^2}$	I

Table 2.1: Conformal Transformations

The eigenvalues of D are $-i\Delta$, where Δ is known as the scaling dimension of the field. Scaling transformations of fields are given by $\phi(x^\mu) \to \lambda^\Delta \phi(\lambda x^\mu)$ [5]. Moreover, the scaling dimension is bound for a four dimensional unitary conformal field theory, with scalars having $\Delta \geq 1$, and vectors having $\Delta \geq 3$ [12].

the Lorentz Algebra. The Poincaré group is an extension of the Lorentz group, which includes translations given by the generators P_μ. The Poincaré algebra can be further extended in two important ways. The first is the conformal algebra, which is the Poincaré algebra plus transformations that preserve angles. The second is the supersymmetry algebra, in which, instead of only considering objects that transform in tensor representations of the Lorentz group, one considers objects that transform in the spinor representation. This introduces $\mathcal{N}$ spinor supercharges, which correspond to $\mathcal{N}$ supersymmetries, and includes anticommutative (fermionic) generators in addition to the preexisting commutative (bosonic) generators [12].

The conformal group has $\mathrm{SO}(2,4) \sim \mathrm{SU}(2,2)$ symmetry, and angle-preserving conformal transformations are given by

$$g_{\mu\nu}(x) \to \Omega^{-2}(x) g_{\mu\nu}(x), \tag{2.12}$$

where the metric $g_{\mu\nu}(x)$ is preserved by an arbitrary positive scale factor [5]. This means that the line element $ds^2 \to (ds')^2 = \Omega^{-2}(x) g_{\mu\nu}(x) dx^\mu dx^\nu$ changes, but angles remain locally unaffected, and importantly, causality is preserved. This extension introduces the generators D for dilatation, K_μ for special conformal transformations as well as inversion symmetry, where the generators obey the conformal algebra. More explicitly, the relevant transformations are given by Table 2.1.

Supersymmetry (SUSY), on the other hand, extends the Poincaré algebra by introducing $\mathcal{N}$ Weyl spinor supercharges, where $\mathcal{N}$ is the number of independent supersymmetries. The SUSY algebra is invariant under rotations of the supercharges into one another, forming the R-symmetry group [14]. The supercharges act as helicity raising and lowering operators on states. For helicity less than 1 (i.e. no gravity) the maximum number of supercharges allowed is $\mathcal{N} = 4$.

The supersymmetric extension of the non-Abelian $\mathrm{SU}(N_c)$ Yang-Mills theory is called $\mathcal{N} = 4$ super Yang-Mills. This is a gauge theory that has superconformal symmetry given by the $\mathrm{SU}(2,2 \mid 4)$ group in four dimensions. Superconformal symmetry includes conformal symmetry, R-symmetry, Poincaré supersymmetry, and conformal supersymmetry. $\mathcal{N} = 4$ SYM has a dimensionless coupling constant g_{YM},

and all fields are massless. It is believed to be UV finite, and has vanishing β functions. Hence, the theory is scale invariant both classically and after quantization. Furthermore, the theory has S-duality group $\mathrm{SL}(2,\mathbb{Z})$ invariance, which is invariance under transformations between strong and weak coupling [12]. These characteristics of $\mathcal{N}=4$ SYM, in combination with its relationship to string theory in the large N_c limit, make it a particularly interesting field theory to study.

2.3 String theory

Conceptually, a relativistic string can be seen as the extension of relativistic point particles to higher dimensions. If a point particle is a zero dimensional object that traces out a one-dimensional worldline in time, then a string is a one-dimensional object that sweeps out a two-dimensional worldsheet in time. Similarly, while the action of the point particle is proportional to the length of the worldline, the action of the string is proportional to the area of the worldsheet. The worldsheet is a Riemann surface, and is parameterized by coordinates that describe its spatial value, and its proper time [15].

Strings come in two types, open and closed, where the open string has two endpoints, and the closed string is a loop with no endpoints. Moreover, strings have a fundamental dimensionful parameter l_s that sets the length scale for the theory, and a fundamental tension given by $T = 1/(2\pi l_s^2)$. The energy of a string scales with its tension T, and its coupling g_s.

The simplest bosonic string theory is described by the Nambu-Goto action, which describes the area of the worldsheet. In this case, equations of motion correspond to extremizing the area of the worldsheet. For the case of open strings, the equation of motion can be solved with Dirichlet or Neumann boundary conditions (BCs). Dirichlet boundary conditions imply that the end point of the string is fixed, while Neumann imply the end point can move.

Perturbative expansion translates nicely from QFT to string theories, in which the topologies of string worldvolumes are expanded out in a similar fashion to Feynman diagrams. In the same spirit, interactions between strings can be included using the coupling constant g_s [12]. Bosonic string theory, however, is only consistent (i.e. not plagued by gauge anomalies) in $d = 26$ dimensions, and contains tachyons.

Such problems can be dealt with by extending string theory to superstring theory via supersymmetry. SUSY ensures that, at any mass level, the bosonic and fermionic degrees of freedom are equal. This introduces fermions, eliminates both closed and open string tachyons, and is consistent in $d = 10$. Quantization of open superstrings gives the Neveau-Schwarz (NS) sector for bosonic states, and the Ramond (R) sector for fermionic states. Closed superstrings are obtained from combinations of open superstrings, and the closed superstring sectors are NS-NS, NS-R, R-NS, and R-R [15].

There are five cases of superstring theories in $d = 10$, but the interesting case with

regard to AdS/CFT is called type IIb superstring theory, which has $\mathcal{N} = 2$ supersymmetry with 32 Poincaré supercharges [16]. Remarkably, the low-energy effective action of Type IIB superstring theory, is the same as that of an independently formulated theory called supergravity (SUGRA), which was acquired by demanding local supersymmetry in general relativity [12]. Classical solutions of SUGRA, known as p-branes, are understood to correspond to the objects on which open strings end, known as D-branes [5].

2.4 D-branes

D-branes were conceived as hyperplanes on which open strings ended when their endpoints were fixed (i.e. Dirichlet boundary conditions). Since their conception, however, D-branes have been extended to dynamical objects that serve a variety of purposes. For example, a string moving freely through spacetime (i.e. Neumann boundary conditions) can be modelled by a spacetime filling D-brane. Moreover, D-branes can have mass, and source closed strings by the worldsheet duality [12].

The dimensions of a D-brane are specified using the Dp-brane notation, where there are p-spatial directions and one time direction. In this way, a D0-brane can be seen as a particle, a D1-brane a string, a D2-brane a sheet, and so on [16]. In contrast to strings, however, D-branes are non-perturbative objects.

The low-energy effective action for massless Dp-branes is acquired by combining the Dirac-Born-Infeld (DBI) action S_{DBI} with Chern-Simons action S_{CS}, yielding $S_{Dp} = S_{DBI} + S_{CS}$. For a single massless brane, S_{DBI} includes pullbacks from NS-NS sector bulk fields, the dilaton, as well as a $U(1)$ gauge field confined to the brane. The Chern-Simons part, on the other hand, includes terms where NS-NS fields couple to background R-R fields, which describes charge under R-R fields on the brane [12]. All in all the full action describes massless excitations of a Dp-brane. Multiple branes can be placed on top of one another, which enhances the gauge field's symmetry from $U(1)$ to $U(N_c)$, where N_c is the number of Dp-branes. Open strings can begin and end on different branes, and the endpoints are kept track of with so-called Chan-Paton factors.

Massive Dp-branes in type IIb superstring theory curve spacetime, and correspond to black p-brane solutions of type IIb SUGRA [5]. Furthermore, they are Bogomol'nyi–Prasad–Sommerfield (BPS) objects that preserve half of the Poincaré supercharges of the background [12]. The importance of such Dp-branes becomes clear in the context of the AdS/CFT correspondence.

2.5 AdS/CFT

The AdS/CFT correspondence identifies objects in $\mathcal{N} = 4$ SU(N_c) SYM field theory with objects in $\mathcal{N} = 2$ Type IIB superstring theory. In addition to being a duality between strong and weak coupling, AdS/CFT is also a duality between open

and closed strings. This can be understood by considering the type IIb superstring theory in flat $\mathbb{R}^{9,1}$ spacetime with a stack of N_c coincident D3-branes embedded in $\mathbb{R}^{3,1}$. The embedding of these D3-branes breaks half of the Poincaré supersymmetry of the string theory. The result is a setup in which open strings begin and end on the D3-branes in $\mathbb{R}^{3,1}$, while closed strings occupy $\mathbb{R}^{9,1}$. The correspondence may be seen by studying two regimes of this system. By first considering weakly coupled open strings at low energies, then strongly coupled closed strings low energies, the relationship between the field theory and the string theory becomes clear [12].

Considering weakly interacting open strings at low energies in the setup described above implies that $g_s \to 0$ and $\alpha' \to 0$. This can be done in such a way that physical observables remain fixed by taking the Maldacena limit, which requires that $u = r/\alpha'$ is fixed as $\alpha' \to 0$ [17]. In this limit, the open and closed strings decouple, and have two differing low-energy effective descriptions. The low-energy effective dynamics of the open strings are given by SU(N_c) $\mathcal{N} = 4$ SYM theory on the worldvolume of the D3-branes in $\mathbb{R}^{3,1}$, while the closed strings are given by type IIb SUGRA in flat $\mathbb{R}^{9,1}$.

On the other hand, considering strongly interacting closed strings at low energies implies that $g_s N_c \to \infty$ and $\alpha' \to 0$ in the initial setup. To begin with, we study the $g_s N_c \to \infty$ limit, where D3-branes become massive and curve the $d = 10$ spacetime. For the extremal case, the $d = 10$ spacetime is is given by the metric

$$ds^2 = H^{-1/2}(-dt^2 + d\vec{x}^2) + H^{1/2}(d\rho^2 + \rho^2 d\Omega_5^2) \tag{2.13}$$

where ρ is the radial coordinate of the background dimensions $\rho^2 = X_4^2 + \ldots + X_9^2$, $H = 1 + \frac{L^4}{\rho^4}$, L is the radius of the space, and $L^4 = 4\pi g_s N_c \alpha'^2$. This metric can be divided into two geometrically distinct regions. The region where $\rho \ll L$ in (2.13) is called the near-horizon region, and is asymptotically $AdS_5 \times S^5$, given by

$$ds^2_{AdS_5 \times S^5} = \frac{\rho^2}{L^2}(-dt^2 + d\vec{x}^2) + \frac{L^2}{\rho^2} d\rho^2 + L^2 d\Omega_5^2, \tag{2.14}$$

while the region $\rho \gg L$ of (2.13), is asymptotically flat $\mathbb{R}^{9,1}$. Then, physical observables are once again fixed by the Maldacena limit as $\alpha' \to 0$. This decouples the closed strings in $d = 10$ space, with the metric (2.13), from the open strings bound to the D3-branes embedded in $\mathbb{R}^{3,1}$.

Clearly, type IIb superstring theory in $\mathbb{R}^{9,1}$, with N_c D3-branes embedded in $\mathbb{R}^{3,1}$, yields very interesting results at low energies. AdS/CFT then serves to relate these objects. More specifically, AdS/CFT states that the on-shell bulk action of type IIb superstring theory in $AdS_5 \times S^5$ corresponds to the generating functional of $\mathcal{N} = 4$ SU(N_c) SYM in $\mathbb{R}^{3,1}$ [17]. This leads to a one-to-one map of states from the string theory in the bulk to the field theory on the boundary. This map relates open strings to closed strings, strongly coupled systems to weakly coupled ones, and is a realization of the holographic principle, as it relates a d dimensional bulk theory to a $d-1$ dimensional boundary theory.

The radial coordinate ρ plays a key role. The near-horizon region $\rho \to 0$ is the UV of the bulk theory, and corresponds to the IR of the boundary theory, while the asymptotic boundary $\rho \to \infty$ is the IR of the bulk theory, and corresponds to the UV of the boundary theory. The bulk theory experiences IR divergences which relate to UV divergences in the boundary theory. These divergences are dealt with by holographic renormalization. This is implemented by first introducing a regulator along the radial coordinate of the bulk action, and constructing covariant counterterms. Then, the holographically renormalized bulk action is acquired by subtracting the counterterms from the regulated action to cancel divergences that appear when removing the regulator [18].

2.6 Geometry

In this section, geometries relevant to this thesis are discussed. First, coordinate systems are described for hyperspheres (section 2.6.1). Then, several relevant coordinate systems for both AdS and dS spacetimes are given (sections 2.6.2 and 2.6.3). Finally, how to foliate AdS with slices of a lower dimensional spacetime is explained with an emphasis on dS_4-sliced AdS_5, where dS_4 is given by static patch coordinates (section 2.6.4).

2.6.1 Spheres

Generally, the sphere S^d may be parameterized by hyperspherical coordinates, which read

$$\begin{aligned} \omega^1 &= \cos\chi_1 \\ \omega^2 &= \sin\chi_1 \cos\chi_2 \\ &\vdots \\ \omega^d &= \sin\chi_1 \dots \sin\chi_{d-1} \cos\chi_d \\ \omega^{d+1} &= \sin\chi_1 \dots \sin\chi_{d-1} \sin\chi_d \end{aligned} \tag{2.15}$$

under the conditions that $0 \leq \chi_i < \pi$ while $1 \leq i < d$, and $0 \leq \chi_d < 2\pi$ [19]. In this way, the line element for S^d may be written as

$$d\Omega_d^2 = d\chi_1^2 + \sin^2\chi_1 d\chi_2^2 + \ldots + \sin^2\chi_1 \dots \sin^2\chi_{d-1} d\chi_d^2. \tag{2.16}$$

When considering the S^5 in $AdS_5 \times S^5$, a convenient form of the line element is

$$d\Omega_5^2 = d\theta^2 + \sin^2\theta d\Omega_{4-i}^2 + \cos^2\theta d\Omega_i^2, \tag{2.17}$$

where $i = 1, 2, 3, 4$ and $0 \leq \theta \leq \pi/2$ [20].

2.6.2 Anti-de Sitter space

In $\mathbb{R}^{2,d}$, anti-de Sitter spacetime (AdS_{d+1}) is given by the hyperboloid

$$X_0^2 - \sum_{i=1}^{d} X_i^2 + X_{d+1}^2 = L^2, \tag{2.18}$$

where L is the AdS radius [12]. The corresponding line element is

$$ds^2 = -dX_0^2 + \sum_{i=1}^{d} dX_i^2 - dX_{d+1}^2. \tag{2.19}$$

One commonly used coordinate system that covers the entire space is called global coordinates. These are given by the parameterization

$$X_0 = L\frac{\cos\tau}{\cos\theta}, \qquad X_i = L\omega_i \tan\theta, \qquad X_{d+1} = L\frac{\sin\tau}{\cos\theta} \tag{2.20}$$

where $i = 1, \ldots, d$ and $\sum_i \omega_i^2 = 1$. Here, τ is a timelike coordinate, θ is a spatial coordinate, and ω_i are angular coordinates for the sphere. This yields the line element

$$ds^2 = \frac{L^2}{\cos^2\theta}(-d\tau^2 + d\theta^2 + \sin^2\theta d\Omega_{d-1}^2), \tag{2.21}$$

with $0 < \theta \leq \frac{\pi}{2}$. A second coordinate system that only covers one half of the space is called Poincaré patch coordinates

$$X_0 = X_4 = \frac{L^2}{2\rho}\left(1 + \frac{\rho^2}{L^4}(-t^2 + \vec{x}^2 + L^2)\right) \qquad X_i = \frac{\rho x_i}{L} \qquad X_5 = \frac{\rho t}{L}, \tag{2.22}$$

where $i = 1, 2, 3$. The corresponding line element reads

$$ds^2_{AdS_5} = \frac{\rho^2}{L^2}(-dt^2 + d\vec{x}^2) + \frac{L^2}{\rho^2}d\rho^2. \tag{2.23}$$

Here, $t \in \mathbb{R}$ is a timelike coordinate, $\rho > 0$ is a radial coordinate, and $x_i = (x_1, x_2, x_3) \in \mathbb{R}^3$ [12]. In these coordinates, the asymptotic boundary is located at $\rho \to \infty$, while the near-horizon region is at $\rho \to 0$. By making the coordinate transformation coordinate transformation $\rho = e^{r/L}$, we acquire a variant of these coordinates, which will be called the r-coordinates

$$ds^2_{AdS_5} = L^2 e^{2r/L}(-dt^2 + d\vec{x}^2) + dr^2. \tag{2.24}$$

Inverting the radial coordinate $\rho = \frac{L^2}{z}$ results in the z-coordinates, which are given by the line element

$$ds^2_{AdS_5} = \frac{L^2}{z^2}(-dt^2 + d\vec{x}^2 + dz^2), \tag{2.25}$$

and the coordinate transformation $z = e^{w/L}$ yields the w-coordinates

$$ds^2_{AdS_5} = L^2 e^{2w/L}(-dt^2 + d\vec{x}^2 + dw^2). \tag{2.26}$$

2.6.3 de Sitter space

In d-dimensions, de Sitter spacetime (dS_d) is given by

$$-X_0^2 + X_1^2 + \ldots + X_d^2 = \ell^2 = \frac{1}{H^2} \tag{2.27}$$

where ℓ is the de Sitter radius, and H is the Hubble constant [6]. Its line element is given by

$$ds^2_{dS_d} = -dX_0^2 + \sum_{i=1}^{d} dX_i^2. \tag{2.28}$$

Similar to AdS, there are also global coordinates in dS that cover the entire space, given by

$$X_0 = \sinh\frac{\tau}{\ell}, \qquad X_i = \Omega_i \cosh\frac{\tau}{\ell}, \tag{2.29}$$

where $\tau \in \mathbb{R}$, $i = 1, \ldots, d$, and $\sum_i \omega_i^2 = 1$. The corresponding line element is

$$ds^2_{dS_d} = -d\tau^2 + \ell^2 \cosh^2\frac{\tau}{\ell} d\Omega^2_{d-1}. \tag{2.30}$$

A second set of coordinates are the static patch coordinates, given by

$$X_0 = \sqrt{\ell^2 - \xi^2}\sinh\frac{\bar{\tau}}{\ell}, \qquad X_j = \xi\Omega_j, \qquad X_d = \sqrt{\ell^2 - \xi^2}\cosh\frac{\bar{\tau}}{\ell} \tag{2.31}$$

where $j = 1, \ldots, d-1$. This yields the line element

$$ds^2_{dS_d} = -\left(1 - \frac{\xi^2}{\ell^2}\right)d\bar{\tau}^2 + \frac{d\xi^2}{1 - \frac{\xi^2}{\ell^2}} + \xi^2 d\Omega^2_{d-2} \tag{2.32}$$

where $\bar{\tau} \in \mathbb{R}$, and $0 \leq \xi < \ell$. Translations in time leave $\bar{\tau}$ unchanged, hence the static nature of the coordinates.

2.6.4 dS_4-sliced AdS_5

An important feature of asymptotically AdS spacetime is that it can be foliated by slices of a lower dimensional spacetime. Consider the asymptotically AdS_d metric G_{MN} where $M, N = 0, 1, \ldots, d$. When expressed in Fefferman-Graham form [21], this reads

$$ds^2_{AdS_d} = G_{MN}(z, x)dX^M dX^N = \frac{L^2}{z^2}(dz^2 + g_{mn}(z, x)dx^m dx^n), \tag{2.33}$$

where $m, n = 0, 1, \ldots, d-1$, and $g_{mn}(z, x)$ is given by the the expansion

$$g_{mn}(z, x) = g^{(0)}_{mn}(x) + z^2 g^{(2)}_{mn}(x) + \ldots + z^d g^{(d)}_{mn}(x) + z^d \log(z^2) h^{(d)}_{mn}(x) + O\left[z^{d+1}\right]. \tag{2.34}$$

The metric at the boundary is then $g_{mn}(0, x) = g^{(0)}_{mn}(x)$. In this context, the flat-slicing is given by $g^{(0)} = \eta$, but it is equally viable to choose dS slicing $g^{(0)} = g_{dS}$. Note that in the interest of computing the 1-point function dual to the scalar slipping

mode, the choice of coordinate system dS is arbitrary. At leading order of the near-boundary expansion (2.34), the line element of dS_4-sliced AdS_5 is then

$$ds^2_{AdS_5} = \frac{L^2}{z^2}(dz^2 + ds^2_{dS_4}), \tag{2.35}$$

Subleading order terms, on the other hand, are computed by using recursively solving Einstein's field equations in a vacuum with a negative cosmological constant under the assumption that $g^{(0)} = g_{dS}$ [22]. This yields the near-boundary expansion at subleading order

$$g_{mn}(z,x) = \left(1 - \frac{z^2}{4\ell^2}\right)^2 g^{dS}_{mn}(x) + O\left[z^4\right], \tag{2.36}$$

which corresponds to the line element

$$ds^2_{AdS_5} = \frac{L^2}{z^2}\left(dz^2 + \left(1 - \frac{z^2}{4\ell^2}\right)^2 ds^2_{dS_4}\right), \tag{2.37}$$

where the asymptotic boundary at $z = 0$, and a bulk horizon exists at $z = 2\ell$. Note that in (2.37), $ds^2_{dS_{d-1}}$ is independent of z-coordinate, which implies that changes in z will only scale the dS space but not affect its internal structure.

Performing the coordinate transformation $z = 2\ell e^{-r/L}$ in the expression (2.37) yields the r-coordinates

$$ds^2_{AdS_5} = \left(\frac{L}{\ell}\right)^2 \sinh^2\left(\frac{r}{L}\right) ds^2_{dS_4} + dr^2, \tag{2.38}$$

where the asymptotic boundary is at $r \to \infty$ and the bulk horizon is at $r \to 0$. In a similar manner, the w-coordinates are acquired through the transformation $z = 2\ell e^{w/L}$, resulting in the line element

$$ds^2_{AdS_5} = \frac{1}{\sinh^2\left(\frac{w}{L}\right)}\left(\left(\frac{L}{\ell}\right)^2 ds^2_{dS_4} + dw^2\right), \tag{2.39}$$

where the asymptotic boundary is at $w \to 0$ and the bulk horizon is at $w \to \infty$ [23].

2.7 Flavor in AdS/CFT

In [4], it was proposed that massive flavors could be added to the gauge theory side of the AdS/CFT correspondence by embedding a small number (N_f) of massive probe D7-branes in the near-horizon geometry of $N_c \to \infty$ D3-branes, given by $AdS_5 \times S^5$ (2.14). The probe D7-brane introduces open string degrees of freedom in the bulk theory, which in the dual picture, corresponds to $\mathcal{N} = 2$ supersymmetric hypermultiplets in the fundamental representation of SU(N_c), in $d = 3 + 1$. On the gravity side, the probe D7-brane breaks half of the supersymmetry of supergravity, leaving eight real Poincaré supercharges. In the dual picture, the $\mathcal{N} = 4$ SYM theory of the couples to an $\mathcal{N} = 2$ hypermultiplet in the fundamental representation of SU(N_c).

Embedding a probe D7-brane in this way allows for open strings connecting the D3- and D7-branes, open strings beginning and ending on the D7 brane, as well as open strings beginning and ending on the D3-branes. If the D7- and D3-branes are separated, the open strings connecting the branes stretch and become massive, breaking the conformal symmetry of the gauge theory. Embedding massive probe D7-branes in this way can lead to a backreaction, in which the mass of the D7-brane distorts the $AdS_5 \times S^5$ geometry to the extent that it is no longer a solution of supergravity. This is dealt with by taking the probe brane limit, in which $N_f \ll N_c$ and $N_f/N_c \to 0$, such that the backreation can be ignored.

In the D3/D7 configuration considered in this thesis, there is a bulk scalar field on the worldvolume of the D7-brane called the slipping mode, that is dual to a boundary operator $\mathcal{O}$, constructed from flavor fields [4]. The mass of the slipping mode is $M^2 = -3$, and although the mass is negative, it is allowed as it is over the Breitenlohner-Freedman bound $M^2L^2 \geq -\frac{d^2}{4}$, where $d = 4$ is the dimension of the gauge theory, and AdS unit radius is used [24]. According to AdS/CFT, the mass on the gravity side M^2 and the dimensions of the dual operator Δ, are related by $M^2L^2 = \Delta(\Delta - d)$, where $\Delta = 1, 3$.

2.7.1 Embedding probe D7-branes in $AdS_5 \times S^5$

In general, the directions in which the branes extend are free Neumann boundary conditions for open strings, while the directions in which the branes do not extend are fixed Dirichlet boundary conditions. Following the prescription of [4], the dimensions occupied by the probe D7-brane, as well as the stack of D3-branes, are chosen as shown in Table 2.3.

	0	1	2	3	4	5	6	7	8	9
D3	×	×	×	×						
D7	×	×	×	×	×	×	×	×		

Table 2.3: The branes extend in the dimensions denoted by ×, and are perpendicular to the remaining dimensions. The 4,5,6,7 directions have a peculiar quality because they are given by Dirichlet boundary conditions for the D3-brane and Neumann boundary conditions for the D7-brane. These are called Neumann-Dirichlet (ND) directions. Note that the D7-brane is parallel to 4,5,6,7 space while the D3-branes are perpendicular to it.

In the bulk theory, the addition of a probe D7-brane breaks the SO(6) isometry of the background dimensions 4,5,6,7,8,9 to SO(4) × SO(2), where the SO(4) acts on $X_4, \ldots, X_7$, and SO(2) acts on X_8 and X_9. In the boundary theory, this corresponds to adding a fundamental hypermultiplet that breaks the SU(4) $\backsimeq$ SO(6) R-symmetry of $\mathcal{N} = 4$ SYM to SO(4) × SO(2). The fundamental hypermultiplet carries opposite charges under SO(2) $\backsimeq$ U(1), and this is viewed as a chiral symmetry [25].

Embedding a probe D7-brane in the near-horizon geometry of the D3-branes is achieved by mapping the 8-dimensional D7-brane embedding coordinates ξ^i, where $i = 0, \ldots, 7$, to the 10-dimensional $AdS_5 \times S^5$ coordinates X^μ, where $\mu = 0, \ldots, 9$. In flat-slicing, with unit AdS radius, the line element of $AdS_5 \times S^5$ reads

$$ds^2 = \frac{1}{z^2}(-dt^2 + d\vec{x}^2 + dz^2) + d\theta^2 + \cos^2\theta d\Omega_3^2 + \sin^2\theta d\psi^2, \tag{2.40}$$

where the S^3 given by $d\Omega_3^2 = d\chi_1^2 + \sin^2\chi_1(d\chi_2^2 + \sin^2\chi_2 d\chi_3^2)$. A convenient choice for the embedding coordinates ξ^i is to simply have them be identical to the first eight coordinates of $AdS_5 \times S^5$. This configuration, called the static gauge, is time independent and preserves the SO(4) symmetry of the S^3.

	0	1	2	3	4	5	6	7
X^μ	t	x_1	x_2	x_3	z	χ_1	χ_2	χ_3
ξ^i	ξ^0	ξ^1	ξ^2	ξ^3	ξ^4	ξ^5	ξ^6	ξ^7

Here, the D7-brane occupies $AdS_5 \times S^3$, filling the dimensions of AdS_5, and wrapping the S^3 inside the S^5. This embedding leaves the 8 and 9 directions unidentified, which are two spherical coordinates of the S^5, namely, the polar angle $X^8 = \theta$, and the azimuthal angle $X^9 = \psi$. Since the D7-brane doesn't extend in these directions, its position is given in 8-9 plane [26].

As long as the D7-brane is located at $(\theta, \psi) = (0, 0)$, it sits exactly on top of the D3-branes, wrapping the S^3 located on the equator of the S^5. At this position, the gravity theory is massless, corresponding to a massless dual theory that preserves conformal symmetry. Furthermore, the SO(2) symmetry of the 8-9 plane is preserved, which corresponds to preserving the U(1) chiral symmetry of the fundamental hypermultiplet in the dual picture.

Making the ansatz that $\psi = 0$ and $\theta = \theta(z)$ allows the D7-brane to move in the θ direction as a function of the radial coordinate z. This choice preserves the translation invariance of the dual theory [20]. The D7-brane being allowed to move in the $\theta(z)$ direction, implies that the S^3 is allowed to move between the equator and the pole of the S^5, located at $\theta = 0$ and $\theta = \frac{\pi}{2}$, respectively. This can be thought of as the higher dimensional analog of a rubber band slipping off a ball. On the gravity side, any nonzero value of θ separates the D3- and D7-branes, giving tension to strings, and breaking the SO(2) symmetry of the 8-9 plane. This gives mass to the field theory, breaks conformal invariance, and breaks the U(1) chiral symmetry of the fundamental hypermultiplet. Note that the distance between the D3- and D7-branes in the θ direction is proportional to the mass of the dual hypermultiplet.

In this thesis, we consider two different ways for the D3- and D7-branes to be separated in the θ direction. The first case involves a cutoff being introduced at a finite value of the radial coordinate $z = z_m$, corresponding to $\theta(z_m) = \frac{\pi}{2}$. In this case, the D7-brane extends along the radial coordinate from the UV at $z = 0$ to the cutoff in the IR at $z = z_m$. This corresponds to S^3 slipping from the equator of the S^5

at $\theta(0) = 0$, to the pole at $\theta(z_m) = \frac{\pi}{2}$, then disappearing from a five-dimensional point of view. Here, the mass of the flavor hypermultiplet can be dialed through the cutoff z_m. In the second case, the position of D7-brane is given by $\theta(0) = \alpha$, where $0 \leq \alpha \leq 2\pi$, implying that the brane extends all the way from the UV to the IR. In this case the mass of the flavor hypermultiplet can be dialed through the cutoff z_m

2.7.2 Scalar slipping mode action

To study the dynamics of $\theta(z)$, we need only consider the pullback of the spacetime metric onto the worldvolume of the D7-brane, which resides in the DBI part of the greater D7-brane action, and reads

$$g_{ij}^{D7} = G_{\mu\nu} \frac{\partial X^\mu}{\partial \xi^i} \frac{\partial X^\nu}{\partial \xi^j}. \tag{2.41}$$

This entails that $\theta(z)$ is contained in an action that is simply proportional to the worldvolume of the brane, which reads

$$\mathcal{S}_{D7} = T_{D7} \int d^8\xi \sqrt{g_{D7}}, \tag{2.42}$$

where $T_{D7} = (2\pi)^{-7} g_s^{-1} (\alpha')^{-4}$, and $g_{D7} = \det(g_{ij}^{D7})$. Notice that this action is of a similar form to the Nambu-Goto action, which is simply proportional to the area of it's worldsheet. The equations of motion resulting from the Nambu-Goto action minimize the area of its 2-dimensional worldsheet, while the equations of motion resulting from (2.42) minimize the worldvolume of the D7-brane. Moreover, the static gauge, and ansatz $\psi = 0$ and $\theta = \theta(z)$, result in considerable simplifications

$$\mathcal{S}_{D7} = T_{D7} \sqrt{g_{S^3}} \sqrt{g_{\mathbb{R}^{1,3}}} \int dz \sqrt{g_{D7}}. \tag{2.43}$$

Here, g_{D7} depends only on z, $\theta(z)$, and $\theta'(z)$, while all other coordinates are integrated out as the volumes of the S^3 and $\mathbb{R}^{1,3}$. Extremizing (2.43) then yields a second-order nonlinear differential equation of motion involving $\theta(z)$. Although the bulk action (2.43) is divergent, it is possible to ensure regular solutions at the level of the boundary conditions of the EOM.

2.7.3 Mapping to flavor fields

AdS/CFT tells us that at the asymptotic boundary, $\theta(z)$ solutions of the bulk EOM yield information about dual operator $\mathcal{O}$. More specifically, as $z \to 0$, the asymptotic behavior of the bulk scalar field is expected to be

$$\theta(z) \sim z^{d-\Delta} \left\{ m + O\left[z^2\right] \right\} + z^{\Delta} \left\{ c + O\left[z^2\right] \right\}, \tag{2.44}$$

where d is the dimension of the gauge theory, Δ is the larger dimension of $\mathcal{O}$, m is the source of $\mathcal{O}$, and c fixes the vacuum expectation value (vev) $\langle \mathcal{O} \rangle$ [12]. The parameters m and c are the leading order coefficients of two series expansions in small

z. For the D3/D7 system, $\Delta = 1, 3$ and $d = 4$, and the leading order asymptotic solution contains a linear and a cubic part

$$\theta(z) = mz + cz^3. \tag{2.45}$$

The linear coefficient m is related to the mass of the hypermultiplet of flavor fields by $m_{\text{true}} = m/(2\pi\alpha')$ [20]. By varying the cutoff $z_m \sim 1/m$, it is possible to dial the mass in the flavor fields. The vev $\langle\mathcal{O}\rangle$, on the other hand, which corresponds to the condensate of the dual flavor fields, is fixed by the leading order linear and cubic coefficients (m and c, respectively) [24].

Given these general expectations of the D3/D7 configuration, we proceed to describe how to compute $\theta(z)$ near the boundary. Consider $AdS_5 \times S^5$, where AdS_5 is given in Fefferman-Graham coordinates (2.33), and the near-boundary expansion (2.34) is to $O\left[z^4\right]$. Computing the pullback of this $AdS_5 \times S^5$ metric to the worldvolume of the D7-brane (2.41), allows one to calculate the slipping mode action (2.43). Expanding the slipping mode action in fluctuations θ about the asymptotic boundary, and retaining only quadratic fluctuation terms, results in a quadratic action. Extremizing the quadratic action then yields a linearized equation of motion, which is subsequently expanded about the asymptotic boundary to $O\left[z^4\right]$. Asymptotic solutions of this this equation of motion will have a general form given in Fefferman-Graham coordinates

$$\theta(z) = z\left\{\sum_{i=0}^{\Delta-1}\alpha_{(i)}z^i + \sum_{j=0}^{\Delta-1}\beta_{(j)}z^j\log(z)\right\} + O\left[z^{\Delta+1}\right]. \tag{2.46}$$

where $\Delta = 3$. The coefficients $\alpha_{(i)}$ and $\beta_{(j)}$ are then determined by the equation of motion. Moreover, the coefficients of (2.46) are expected to simplify such that the leading order cubic and linear coefficients ($\alpha_{(0)}$ and $\alpha_{(2)}$) determine all others. If this is the case, then these coefficients have been identified as the mass and condensate parameters m and c, as shown in (2.44).

For the flat-slicing of the D3/D7 scalar slipping mode, where AdS is given by (2.25), an exact solution to the bulk EOM is known to be

$$\theta(z) = \arcsin(mz) = mz + \frac{m^3}{6}z^3 + \ldots, \tag{2.47}$$

where cutoff is located at $z_m = 1/m$, and the condensate relates to the mass by $c(m) = \frac{m^3}{6}$. This is referred to as the supersymmetric background solution, and will act as a benchmark as it is identified with $\langle\mathcal{O}\rangle = 0$ [24].

3
Flat Case

In the flat case, the equation of motion of the D3/D7 scalar slipping mode in flat-slicing is solved numerically, and the values corresponding to the dual mass and condensate are extracted from the numerical solution. In section 3.1, a massive probe D7-brane with flavor is embedded in the $AdS_5 \times S^3$ subspace of $AdS_5 \times S^5$, where AdS_5 is foliated by slices of Minkowski space. Then, the action and equation of motion are calculated. Thereafter, in section 3.2, holographic renormalization is implemented at the level of the boundary conditions. In section 3.3, the EOM is solved using a numerical differential equation solver and the holographically renormalized boundary conditions. For the flat-slicing, the EOM is known to be solved by the supersymmetric background solution, and a solution with the form of (2.47) is used as a fitting function for the numerical solution. Finally, the numerically computed coefficients corresponding to the mass and condensate are plotted and compared to the background solution. This is in order to confirm that the embedding, boundary conditions, and numerical solver are all functioning correctly.

3.1 Probe D7-brane in flat-slicing

The line element of $AdS_5 \times S^5$ reads

$$ds^2_{AdS_5\times S^5} = G_{MN}dX^M dX^N = ds^2_{AdS_5} + d\Omega_5^2 \tag{3.1}$$

where X^M are coordinates in $d = 10$ with $M, N = 0, \ldots, 9$. For the flat case, AdS_5 is foliated by slices of Minkowski space $\mathbb{R}^{3,1}$, which reads

$$ds^2_{AdS_5} = \frac{1}{z^2}\left(ds^2_{\mathbb{R}^{3,1}} + dz^2\right) = \frac{1}{z^2}\left(-dt^2 + d\vec{x}^2 + dz^2\right), \tag{3.2}$$

where $\vec{x} = (x_1, x_2, x_3)$. The S^5 on the other hand, is expressed in the same coordinates as (2.17), reading

$$d\Omega_5^2 = d\theta^2 + \cos^2\theta d\Omega_3^2 + \sin^2\theta d\psi^2 \tag{3.3}$$

where $d\Omega_3^2 = d\chi_1^2 + \sin^2(\chi_1^2)(d\chi_2^2 + \sin^2(\chi_2)d\chi_3^2)$. The flat-slicing of $AdS_5 \times S^5$ is then

$$ds^2_{AdS_5\times S^5} = \frac{1}{z^2}(-dt^2 + d\vec{x}^2 + dz^2) + d\theta^2 + \cos^2\theta d\Omega_3^2 + \sin^2\theta d\psi^2. \tag{3.4}$$

In these coordinates, the asymptotic boundary is located at $z = 0$ and the near-horizon region is at $z \to \infty$. The induced metric of $AdS_5 \times S^5$ onto the worldvolume of the D7-brane, can be acquired from (3.4) using (2.41), which reads

$$ds^2_{D7} = G_{MN}\frac{\partial X^M}{\partial \xi^i}\frac{\partial X^N}{\partial \xi^j}d\xi^i d\xi^j = g^{D7}_{ij}d\xi^i d\xi^j, \tag{3.5}$$

where ξ^i are the embedding coordinates, and $i, j = 0, \ldots, 7$. The choice of embedding is the static gauge where the embedding coordinates are identified as

$$(\xi^0, \xi^1, \xi^2, \xi^3) = (t, x_1, x_2, x_3),\ \xi^4 = z,\ (\xi^5, \xi^6, \xi^7) = (\chi_1, \chi_2, \chi_3). \tag{3.6}$$

The remaining two coordinates X^8 and X^9 are chosen to be $(X^8, X^9) = (\theta, \psi)$, which implies that the D7-brane's position in $AdS_5 \times S^5$ space is given in the (θ, ψ) plane. The ansatz is then made that $\psi = 0$ and $\theta = \theta(z)$, such that the brane is only free to move in the θ direction as a function of the radial coordinate z. Computing the induced metric under these assumptions gives

$$g^{D7}_{ij} = \mathrm{diag}\{-G_{00}, \ldots, G_{77}\} + G_{88}\partial_i X^8 \partial_j X^8 + G_{99}\partial_i X^9 \partial_j X^9. \tag{3.7}$$

Due to the ansatz, the $G_{88}\partial_i X^8 \partial_j X^8$ term gives a non-zero contribution, while the $G_{99}\partial_i X^9 \partial_j X^9$ term is zero, yielding the line element

$$ds^2_{D7} = \frac{1}{z^2}ds^2_{\mathbb{R}^{3,1}} + \left(\frac{1}{z^2} + \left(\frac{\partial\theta(z)}{\partial z}\right)^2\right)dz^2 + \cos^2\theta(z)d\Omega^2_3. \tag{3.8}$$

Given the explicit form of the induced metric, it is possible to compute an action. The dynamics of the of the scalar slipping mode are given by an action that is simply proportional to the volume of the brane, which reads

$$\mathcal{S}_{D7} = T_{D7}\int d\xi^8 \sqrt{g_{D7}}. \tag{3.9}$$

where $g_{D7} = \det g^{D7}_{ij}$. Inserting the induced metric (3.8) into the action (3.9), then performing the integration over the $\mathbb{R}^{3,1}$ and S^3 coordinates, yields the volumes of the respective spaces. As $\sqrt{g_{\mathbb{R}^{3,1}}}$, $\sqrt{g_{S^3}}$, and T_{D7} are simply constant, they are suppressed from the calculation. The part of the action with $\theta(z)$ dependence is then

$$\tilde{\mathcal{S}}_{D7} = \int dz \frac{\cos^3\theta(z)}{z^5}\sqrt{1 + z^2\left(\frac{\partial\theta(z)}{\partial z}\right)^2}. \tag{3.10}$$

Extremizing the action (3.10) with respect to $\theta(z)$ yields the second-order nonlinear equation of motion for the slipping mode in flat slicing

$$z\cos(\theta(z))\left(4z^2\theta'(z)^3 - z\theta''(z) + 3\theta'(z)\right) - 3\left(z^2\theta'(z)^2 + 1\right)\sin(\theta(z)) = 0. \tag{3.11}$$

To ensure that the near-boundary behavior in flat slicing is indeed given by (2.47), one simply needs to perform the near-boundary expansion on action (3.10), and find the resulting solution. By expanding the action about the boundary to subleading order in θ, and retaining only quadratic terms, one arrives at the linearized EOM

$$\frac{\theta''(z)}{z^3} - \frac{3\theta'(z)}{z^4} + \frac{3\theta(z)}{z^5} = 0. \tag{3.12}$$

Here, assuming a solution of the form $\theta(z) = z^{\Delta}$ yields $\Delta = 1, 3$, which confirms the scaling dimensions suggested in section 2.7. Moreover, assuming an asymptotic solution of the general form (2.46) with $\Delta = 3$, results in the background solution (2.47)

$$\theta(z) = mz + \frac{m^3}{6}z^3 + O\left[z^4\right]. \tag{3.13}$$

3.2 Holographic renormalization

To solve the equation of motion (3.11), boundary conditions are constructed using tools from holographic renormalization in order to deal with the divergent boundaries. Two types of IR boundary conditions will be discussed. The first case involves the D7-brane extending from the UV boundary ($z = 0$) and ending at a cutoff at a finite $z = z_m$, while the second case involves the D7-brane extending all the way to the IR boundary ($z = \infty$).

First, however, note that embedding the D7-brane in the $AdS_5 \times S^3$ subspace of $AdS_5 \times S^5$ implies that it occupies all of dimensions AdS_5, and wraps the S^3 inside the S^5. Generically, for the slipping mode, the D7-brane is free to move in the θ direction, between the equator and the pole of the S^5 at $\theta = 0$ and $\theta = \frac{\pi}{2}$, respectively. The massless case is given by the D7-brane being located at $\theta = 0$, where there is no separation between the D3- and D7-branes. The massive case, on the other hand, is given by $0 < \theta \leq \frac{\pi}{2}$.

The cutoff boundary conditions are constructed by having the S^3 slip off the pole of the S^5 at the cutoff $z = z_m$, corresponding to $\theta(z_m) = \frac{\pi}{2}$. Moreover, the generic condition in the UV is given by the massless case $\theta(0) = 0$. Together, these yield the generic cutoff conditions

$$\begin{aligned} \theta(z = 0) &= 0, \\ \theta(z = z_m) &= \frac{\pi}{2}, \end{aligned} \tag{3.14}$$

where the D7-brane occupies $0 \leq z \leq z_m$. These boundary conditions yield a two parameter family of divergent solutions of the EOM (3.11), where the divergences are associated with the boundaries.

To remove the divergences at the boundaries, a regulator (ϵ) is introduced, where $\epsilon \ll 1$, such that the boundaries are avoided when solving (3.11). This results in the modification

$$\begin{aligned} \theta(z = \epsilon) &= \epsilon, \\ \theta(z = z_m) &= \frac{\pi}{2} - \epsilon. \end{aligned} \tag{3.15}$$

The cutoff $z = z_m$, however, must be considered in more detail. Here, a divergence occurs because the D7-brane doesn't end smoothly due to a singularity occurring when the S^3 slips off the pole of the S^5. To understand this, we can recall the analogy that the S^3 wrapping the S^5 is somewhat like a rubber band wrapping a ball.

At $\theta = 0$, the S^3 wraps the equator of the S^5. As θ increases, the S^3 travels toward the pole at $\theta = \frac{\pi}{2}$, shrinking along the way. Upon reaching the pole, the shrinking S^3 contracts to zero, which results in a conical singularity. This divergence can be avoided by demanding that instead of contracting to zero, the S^3 shrinks smoothly, resulting in Euclidean space at the pole.

To illustrate how a sphere can shrink to Euclidean space, consider the round metric on a 4-sphere $ds^2 = dr^2 + \sin^2 r d\Omega_3^2$, where the S^3 is shrinking as a function of the radial coordinate r. Taking $r \to 0$ allows one to approximate $\sin^2 r \approx r^2$, yielding $ds^2 = dr^2 + r^2 d\Omega_3^2$, which is nothing other than 4-dimensional Euclidean space in spherical coordinates. Such smooth shrinking can be implemented in the slipping mode via a substitution of variables. To realize this, we substitute $\theta(z) = \frac{\pi}{2} - \varphi(z)$, where $\varphi(z = 0) = \frac{\pi}{2}$ and $\varphi(z = z_m) = 0$, in the induced metric (3.8), yielding the line element

$$ds_{D7}^2 = \frac{1}{z^2} ds_{\mathbb{R}^{3,1}}^2 + \left(1 + \frac{1}{z^2}\left(\frac{\partial z}{\partial \varphi}\right)^2\right) d\varphi^2 + \sin^2 \varphi(z) d\Omega_3^2. \tag{3.16}$$

Then, by requiring $\frac{dz}{d\varphi} = 0$ at $z = z_m$, the shrinking S^3 results in Euclidean space as $z \to z_m$

$$ds_{D7}^2 = d\varphi^2 + \varphi^2 d\Omega_3^2 + \dots. \tag{3.17}$$

This can be recast as $\theta'(z_m) = \infty$, yielding new IR boundary conditions at the cutoff that ensure the smooth shrinking of the S^3 at the pole of the S^5

$$\begin{aligned} \theta(z = z_m) &= \frac{\pi}{2} - \epsilon, \\ \theta'(z = z_m) &= \Lambda, \end{aligned} \tag{3.18}$$

where $\Lambda = \frac{1}{\epsilon}$. The second case is where the D7-brane extends all the way to the IR boundary, requiring new boundary conditions at $z = \infty$. Clearly, the z-coordinates aren't the convenient for this region, so the r-coordinates are used instead, where the IR boundary is located at $r = 0$. Here, we consider a new way to separate the D3- and D7-branes in the θ direction. This is implemented by the conditions

$$\begin{aligned} \theta(r = 0) &= \alpha, \\ \theta'(r = 0) &= 0, \end{aligned} \tag{3.19}$$

where α is dialed between $0 \leq \alpha \leq 2\pi$, and the massless case is given by $\alpha = 0$. Here, divergences are once again handled by introducing the regulator ϵ, resulting in the modified conditions

$$\begin{aligned} \theta(r = \epsilon) &= \alpha, \\ \theta'(r = \epsilon) &= \epsilon. \end{aligned} \tag{3.20}$$

3.3 Numerics in flat-slicing

The numerical differential equation solver NDsolve (Mathematica) is used to solve the EOM (3.11), using the cutoff boundary conditions (3.18), where the parameters

were chosen to be $z_m = 1$, $\epsilon = 10^{-3}$, and $\Lambda = 10^3$. The solution was then plotted against the supersymmetric background solution (2.47) to confirm that the NDsolve was functioning properly (Fig. 3.1a).

Thereafter, the relationship between m and c was studied at various values of the cutoff z_m, corresponding to dialing the mass in the dual picture. Note that the cutoff z_m is inversely proportional to the mass. This was realized by a For-loop containing NDsolve, which iterated through 20 different values of z_m between $0.1 \leqslant z_m \leqslant 2$, solving the EOM (3.11) each time. Each solution was fit to a function $f_{\text{fit}}(z)$ containing a linear and cubic part

$$f_{\text{fit}}(z) = mz + cz^3. \tag{3.21}$$

The coefficients (m, c) were then collected from the fitting function (3.21) and plotted, as depicted in Figure 3.1b. As a confirmation of the mass and condensate being extracted from NDsolve correctly, the supersymmetric background solution $c(m) = \frac{m^3}{6}$ was expected to be reproduced each time.

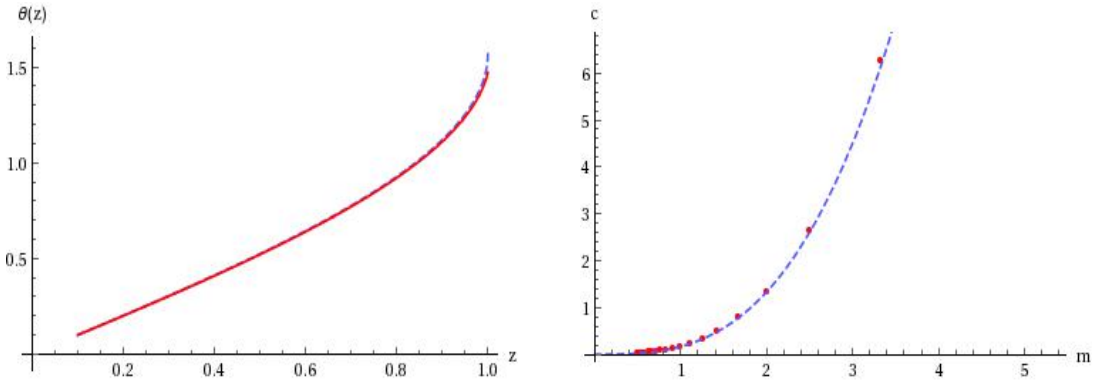

(a) **(b)**

Figure 3.1: (a) Numerically computed $\theta(z)$ in flat slicing (solid red line) versus background solution $\arcsin(mz)$ (dashed blue line). (b) Mass and condensate parameters (m, c) (solid red dots) versus background solution $c(m) = m^3/6$ (dashed blue line). This confirms that the numerics are working properly and that a probe D7-brane has been embedded into $AdS_5 \times S^5$ in flat-slicing.

4

Curved Case

4.1 Probe D7-brane in dS_4-sliced AdS_5

In section 4.1.1, the probe D7-brane is embedded in the $AdS_5 \times S^3$ subspace of $AdS_5 \times S^5$, where AdS_5 is foliated by slices of dS_4 according to section 2.6.4. The boundary asymptotics of the slipping mode are discussed in section 4.1.2, and the mass and condensate are identified in section 4.1.3. In section 4.2, the slipping mode equation of motion is solved numerically and fit to the asymptotic solution in order to numerically compute the mass and condensate. Thereafter, in section 4.3, the correction to the mass is computed analytically and shown to accurately describe medium mass slipping mode solutions.

4.1.1 Embedding

For dS_4-sliced AdS_5, the line element of $AdS_5 \times S^5$ expressed in the w-coordinates reads

$$ds^2_{AdS_5\times S^5} = \frac{1}{\sinh^2(\frac{w}{L})}\left(\left(\frac{L}{\ell}\right)^2 ds^2_{dS_4} + dw^2\right) + L^2(d\theta^2 + \cos^2\theta d\Omega_3^2 + \sin^2\theta d\psi^2), \quad (4.1)$$

Here, the asymptotic boundary is located at $w = 0$, and a horizon exists at $w = \infty$. We proceed by setting $L = \ell = 1$. The line element of the D7-brane is then

$$ds^2_{D7} = \frac{1}{\sinh^2(w)} ds^2_{dS_4} + \left(\frac{1}{\sinh^2(w)} + \left(\frac{\partial\theta(w)}{\partial w}\right)^2\right) dw^2 + \cos^2\theta(w) d\Omega_3^2, \quad (4.2)$$

corresponding to the slipping mode action

$$\tilde{\mathcal{S}}_{D7} = \int dw \frac{\cos^3\theta(w)}{\sinh^5(w)} \sqrt{1 + \sinh^2(w)\left(\frac{\partial\theta(w)}{\partial w}\right)^2}, \quad (4.3)$$

Notice that this action is the same as (3.10) with the z terms in the argument replaced with $\sinh(w)$. Moreover, in both the w- and z- coordinates asymptotic boundaries are located at zero, and at leading order, expanding in small w gives $\sinh(w) \approx w$. These observations will be used when performing the near-boundary

expansion. Extremizing the action (4.3) results in the second order non-linear equation of motion for the slipping mode

$$\begin{aligned}\operatorname{csch}(w)\left(\theta''(w)\cos(\theta(w))+3\sin(\theta(w))\left(\theta'(w)^2+\operatorname{csch}^2(w)\right)\right)\\ -\cosh(w)\theta'(w)\cos(\theta(w))\left(4\theta'(w)^2+3\operatorname{csch}^2(w)\right)=0.\end{aligned} \tag{4.4}$$

4.1.2 Asymptotic solutions

AdS/CFT tells us that the mass and condensate of the dual hypermultiplet is given by the form of bulk scalar solutions $\theta(w)$ near the asymptotic boundary of AdS at $w = 0$. More specifically, by solving the near-boundary expansion of the EOM with power series solutions $\theta(w)$, it is possible to identify the mass and condensate of the dual theory as coefficients. Studying near-boundary behavior can be cumbersome in w-coordinates. Given that both the w- and z-coordinates have the asymptotic boundary of AdS located at zero, and that solutions θ will behave the same in this limit, switches will be made between w and z. In z-coordinates, asymptotic solutions are expected to have the form

$$\theta(z) \to z^{d-\Delta}\left\{m + O\left[z^2\right]\right\} + z^{\Delta}\left\{c + O\left[z^2\right]\right\}. \tag{4.5}$$

where Δ is the larger dimension of the dual operator $\mathcal{O}$ (larger root of $M^2L^2 = \Delta(\Delta - d)$), the dimension of the boundary theory is d, the mass of $\mathcal{O}$ is proportional to m, and its vev $\langle\mathcal{O}\rangle$ is fixed by c. For the D3/D7 system, $\Delta = 3$, $d = 4$, m is proportional to the mass of a fundamental hypermultiplet of flavor fields, and its chiral condensate is fixed by c. The results is a solution containing a linear part $z^{d-\Delta} = z$, and a cubic part $z^{\Delta} = z^3$, where m and c are the leading order coefficients of two independent series solutions. This implies that at leading order in the near-boundary expansion, the asymptotic solution is expected to be

$$\theta(z) = mz + cz^3, \tag{4.6}$$

At higher orders, however, there is the possibility of mixed terms. This can be seen by considering the first few orders of a power series solution (2.46) in the z-coordinates

$$\theta(z) = z\left\{\alpha_{(0)} + \alpha_{(1)}z + \alpha_{(2)}z^2 + \beta_{(2)}z^2\log(z) + \ldots\right\} + z^3\left\{\bar{\alpha}_{(0)} + \ldots\right\}, \tag{4.7}$$

where both $\alpha_{(2)}$ and $\bar{\alpha}_{(0)}$ are cubic coefficients. The consequence leaving this mixing unsolved is that the cubic coefficient of a fitting function in the numerical routine would contain contributions that don't pertain to the condensate. To sort this out, the contributions to the cubic coefficient may be identified analytically by solving the near-boundary expansion of the EOM with power series solutions. The near-boundary expansion is performed first by expanding in small $\theta(w)$ in the action (4.3), then retaining only quadratic terms results in a linearized EOM near the boundary. Thereafter, an expansion is performed in small w, and coordinates are switched to z, where the cubic z^3 term is studied to assess whether there is an $\alpha_{(2)}$ contribution. In accordance with [24], asymptotic solutions are expected to only contain of odd powers of z ($\alpha_{(1)} = \alpha_{(3)} = \ldots = 0$), and logarithmic terms are expected to only occur only after subleading order ($\beta_{(0)} = \beta_{(1)} = 0$).

4.1.3 Near-boundary expansion

Expanding the argument of the action (4.3) to subleading order in $\theta(w)$ yields

$$\tilde{\mathcal{S}}_{D7} \approx \int dw \frac{1}{\sinh^5(w)} \left(1 - \frac{3\theta(w)^2}{2}\right) \left(1 + \sinh^2(w) \frac{\theta'(w)^2}{2}\right) \tag{4.8}$$

where considering only quadratic terms implies

$$\tilde{\mathcal{S}}_{D7} \approx \int dw \left(-\frac{3\theta(w)^2}{2\sinh^5(w)} + \frac{\theta'(w)^2}{2\sinh^3(w)}\right). \tag{4.9}$$

When extremized with respect to $\theta(w)$, yields a linearized equation of motion

$$\frac{\theta''(w)}{\sinh^3(w)} - \frac{3\cosh(w)\theta'(w)}{\sinh^4(w)} + \frac{3\theta(w)}{\sinh^5(w)} = 0. \tag{4.10}$$

The near-boundary expansion of (4.10) then proceeds by expanding $\cosh(w)$ and $\sinh(w)$ to subleading order in power series about $w = 0$ results in

$$\frac{\theta''(w)}{\left(w + \frac{z^3}{6}\right)^3} - \frac{3\left(1 + \frac{w^2}{2}\right)\theta'(w)}{\left(w + \frac{w^3}{6}\right)^4} + \frac{3\theta(w)}{\left(w + \frac{w^3}{6}\right)^5} = 0. \tag{4.11}$$

Simplification yields that at leading (4.12) and subleading (4.13) orders of the near-boundary expansion, the equation of motion reads

$$0 = \frac{\theta''(w)}{w^3} - \frac{3\theta'(w)}{w^4} + \frac{3\theta(w)}{w^5}, \tag{4.12}$$

$$0 = \left(\frac{1}{w^3} - \frac{1}{2w}\right)\theta''(w) + \left(\frac{3}{w^5} - \frac{5}{2w^3}\right)\theta(w) + \left(\frac{2}{w^2} - \frac{3}{w^4}\right)\theta'(w) \tag{4.13}$$

The first equation (4.12) is identical to the linearized flat-slicing EOM (3.12) near the boundary of AdS. This is expected because at leading order of the near-boundary expansion, (2.35), there is no correction for the curvature of de Sitter space. Equation (4.13), on the other hand, is the linearized EOM near the boundary of AdS in dS_4-sliced AdS_5 given by the metric (2.37). To identify whether the cubic term in the full asymptotic solution (4.7) contains a contribution that doesn't pertain to the condensate ($\alpha_{(2)}$), we insert the solution

$$\theta(w) = \alpha_{(0)} w + \alpha_{(1)} w^2 + \alpha_{(2)} w^3 + \beta_{(2)} w^3 \log(z) + O\left[w^4\right], \tag{4.14}$$

into the near-boundary expansion EOM. For the dS-slicing EOM (4.13), the coefficients are identified as $\alpha_{(1)} = \alpha_{(2)} = 0$ and $\beta_{(2)} = \frac{1}{4}\alpha_{(0)}$. As a check, the coefficients in the flat-slicing EOM (4.12), were identified as $\alpha_{(1)} = \beta_{(2)} = 0$, and the solution is the supersymmetric background solution, as expected. Given that $\alpha_{(2)} = 0$ in dS-slicing, it can be concluded that there is no mixing of terms in the cubic coefficient of the full asymptotic solution. In terms of the mass and condensate parameters, the asymptotic solution then reads

$$\theta(w) = mw + cw^3 + \frac{1}{4} m w^3 \log(z) + O\left[w^4\right] \tag{4.15}$$

4.2 Numerics in dS_4-sliced AdS_5

The numerical differential equation solver NDsolve was used to iteratively solve the EOM (4.4) at different cutoffs, using the cutoff boundary conditions (3.18), with $\epsilon = 10^{-3}$ and $\Lambda = 10^3$. The computation was done in the z-coordinates (2.37), where the dS-horizon is located at $z = 2\ell$, and we set $\ell = 1$. This was once more implemented by a For-loop, containing NDsolve, which iterated through 20 different values of z_m. Each numerical solution was fit to a function with the form of the analytically acquired solution (4.15)

$$f_{\text{fit}}(z) = mz + \frac{1}{4}mz^3 \log(z) + cz^3, \tag{4.16}$$

in a fitting window between $\epsilon \leq z \leq 5\epsilon$. The coefficients (m, c) were then collected from the fitting function (4.16) and plotted. In order to study the large and small mass limits, the interval of iteration was changed for the cutoff z_m.

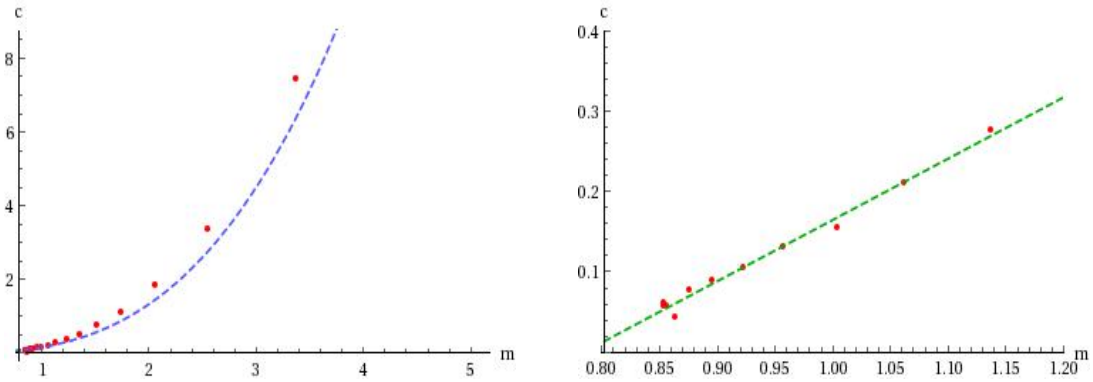

(a) **(b)**

Figure 4.1: (a) Small mass solutions in dS_4-slicing (red dots) versus flat-space solution $c(m) = m^3/6$ (blue line) in the interval $z_m = \{0.099, 1.980\}$. The numerical solutions appears to be off-set from the flat-space solution. (b) Close-up view of smallest values in (a) where the solution was found to be approximately linear $c(m) \approx 0.76m$ (green line). At the smallest masses, near the cutoff $z_m = 2$, the numerical solver hits the dS-horizon.

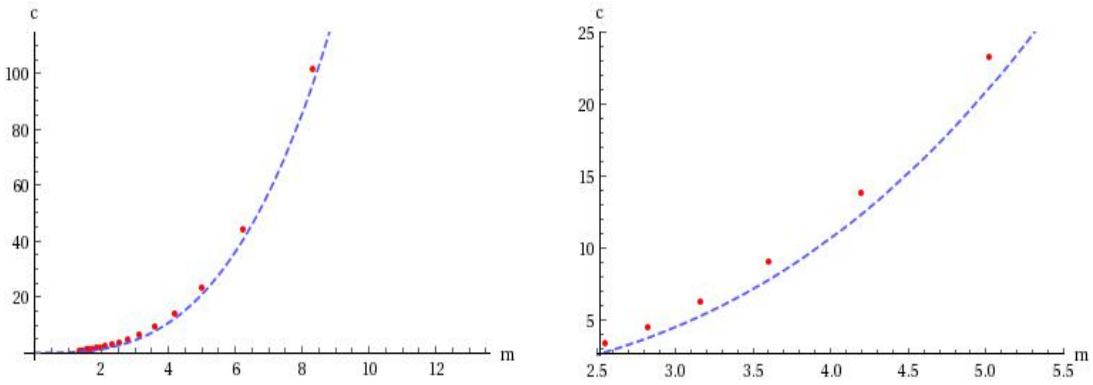

(a) **(b)**

Figure 4.2: (a) Medium mass solutions in dS_4-slicing (red dots) versus flat-space solution $c(m) = m^3/6$ (blue line) in the interval $z_m = \{0.04, 0.8\}$. (b) Close-up view of (a). Again, the numerical solution appears to be off-set from the flat-space solution.

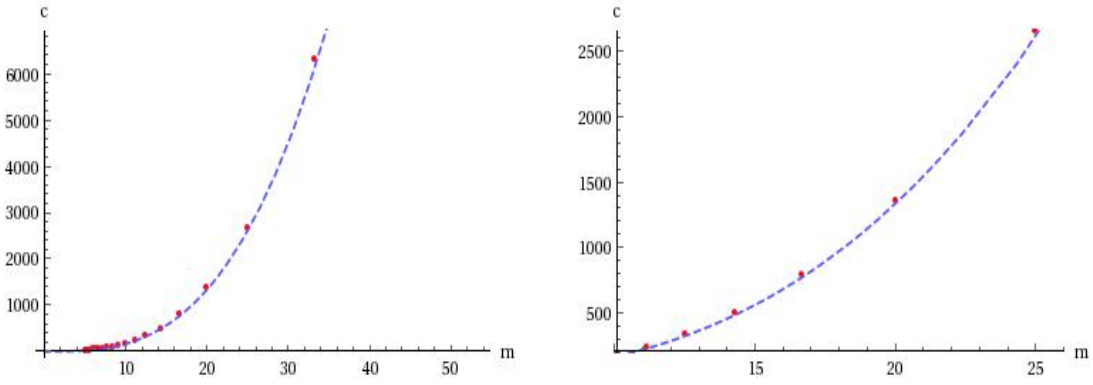

(a) **(b)**

Figure 4.3: (a) Large mass solutions in dS_4-slicing (red dots) versus flat-space solution $c(m) = m^3/6$ (blue line) in the interval $z_m = \{0.01, 0.2\}$. (b) Close-up view (a). The numerical solution appears to follow the flat-space solution.

At the smallest masses, the relationship between the numerically computed parameters m and c was found to be approximately linear ($c(m) \approx 0.76m$). Masses could not be computed beyond the cutoff $z_m = 2$, as the numerical solver hit the de Sitter horizon at $z = 2\ell$. As the mass gets larger, the numerical solution appears to follow the flat-space solution $c(m) = m^3/6$ in an offset manner, while at the largest masses, the numerical solver clearly reproduces the flat-space solution.

At small masses $m \ll \frac{1}{\ell}$, the effects of de Sitter curvature to dominate the relationship between the mass and condensate parameters m and c. Moreover, the smallest mass solutions are hidden behind the de Sitter horizon, and acquiring them requires a change of coordinates. At large masses $m \gg \frac{1}{\ell}$, the effects of de Sitter curvature become negligible in comparison to the effects of the mass. This is confirmed by the reappearance of the flat-space solution. At medium masses, however, there

appears to exist a regime in which both the effects of dS curvature and mass are non-negligible. Accurately describing this region requires a correction to the mass.

4.3 Mass correction

To determine the relationship between the mass and condensate in the medium mass regime, where the effects of both dS curvature and mass are non-negligible, the correction to the mass is calculated. This is accomplished by performing a large mass expansion in small values of the inverse de Sitter radius $\frac{1}{\ell}$. In this case, the dS-radius is no longer suppressed from the slipping mode action

$$\tilde{\mathcal{S}}_{D7} = \int dz \frac{1}{z^5}\left(1-\frac{\lambda^2 z^2}{4}\right)\cos^3\theta(z)\sqrt{1+z^2\left(\frac{\partial\theta(z)}{\partial z}\right)^2}, \tag{4.17}$$

where $\lambda = \frac{1}{\ell}$. Computing the equation of motion of (4.17), then expanding about $\lambda = 0$ up to order $O\left[\lambda^4\right]$ results in the expression

$$\begin{aligned} z\cos(\theta(z))\left(z\left(4-\lambda^2 z^2\right)\theta''(z)+2z^2\left(\lambda^2 z^2-8\right)\theta'(z)^3+\left(\lambda^2 z^2-12\right)\theta'(z)\right) \\ -3\left(\lambda^2 z^2-4\right)\left(z^2\theta'(z)^2+1\right)\sin(\theta(z))=0. \end{aligned} \tag{4.18}$$

In this case, solutions of the EOM have the form

$$\theta(z) = \theta_{(0)}(z) + \lambda^2\theta_{(2)}(z) + O\left[\lambda^4\right] \tag{4.19}$$

where $\theta_{(0)}(z) = mz + \frac{m^3}{6}z^3 + O\left[z^4\right]$ is the flat-space solution (2.47), and $\theta_{(2)}(z)$ is to be determined. Applying the cutoff boundary conditions (3.18) to $\theta(z)$ results in additional conditions for the leading and subleading order solutions

$$\begin{aligned} \theta_{(0)}(z_m) &= \frac{\pi}{2}, \qquad & \theta'_{(0)}(z_m) &= \infty, \\ \theta_{(2)}(z_m) &= 0, \qquad & \theta'_{(2)}(z_m) &= 0. \end{aligned} \tag{4.20}$$

Inserting the solution (4.19) into the EOM (4.18), expanding in a series up to $O\left[\lambda^4\right]$, and solving with Dsolve yields a solution $\theta_{(2)}(z)$ that is dependent on two undetermined constants. These constants are identified by expanding $\theta_{(2)}(z)$ to leading order about the $z = z_m$ boundary and applying the boundary condition $\theta_{(2)}(z_m) = 0$. To fourth order in z, the solution $\theta(z)$ then reads

$$\begin{aligned} \theta(z) = &\left(\frac{1}{z_m}+\lambda^2\frac{z_m}{8}+O\left[\lambda^4\right]\right)z \\ &+\left(\frac{1}{6z_m^3}+\lambda^2\left(\frac{1}{16z_m}-\frac{\log(z_m)}{4z_m}+\frac{\log(z)}{4z_m}\right)+O\left[\lambda^4\right]\right)z^3 \end{aligned} \tag{4.21}$$

The corrected field theory parameters (m and c) were reinstated in (4.21) by demanding that the linear z coefficient should be the corrected mass m, which is accomplished by $z_m = \frac{1}{m}\left(1+\lambda^2\frac{1}{8m^2}\right)$. In terms of the physical mass and condensate,

the leading order correction then reads

$$\theta(z) = mz + \left(\frac{m^3}{6} + \lambda^2 \frac{1}{4} m \log(mz)\right) z^3 + O\left[z^4\right], \tag{4.22}$$

where the corrected condensate is identified as the cubic coefficient $c(m) = \frac{m^3}{6} + \lambda^2 \frac{1}{4} m \log(m)$.

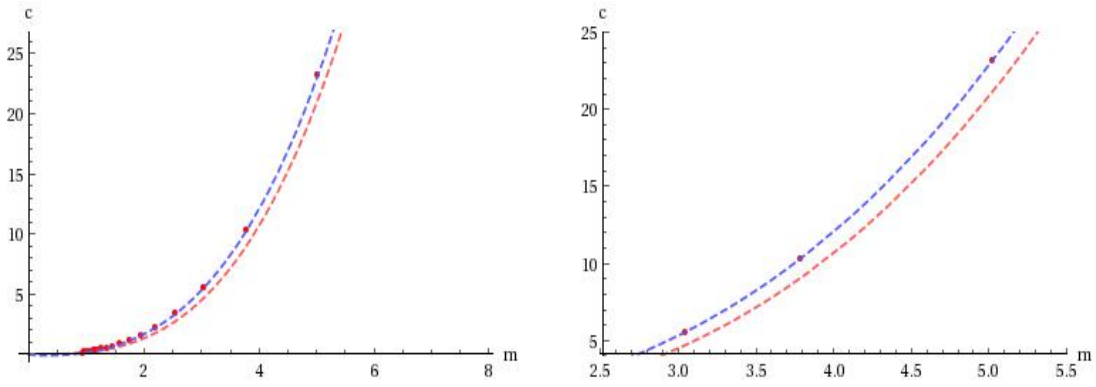

(a) **(b)**

Figure 4.4: (a) Medium mass solutions in dS_4-slicing (red dots), mass correction $c(m) = \frac{m^3}{6} + \lambda^2 \frac{1}{4} m \log(m)$ (blue line), uncorrected flat space solution $c(m) = m^3/6$ (red line) in the interval $z_m = \{0.06, 1.33\}$. (b) Close-up view of (a). The correction to the mass clearly fixes offset of the uncorrected flat-space solution.

4.4 Behind the horizon

Switching to r-coordinates (2.38) allows one to obtain the smallest mass solutions that have up until this point been located behind the horizon. Moreover, the linear behavior of the smallest mass solutions can be evaluated analytically. Finally, in these coordinates it is possible to consider new embedding in which the D7-brane extends to the center of AdS. In section 4.4.1, the embedding of a probe D7-brane is described in r-coordinates. In section 4.4.2, the form of the asymptotic solution in the new coordinates is confirmed, and the form of the near-massless solutions are evaluated using the IR boundary conditions (3.20). Finally, in section 4.5, the slipping mode EOM is solved for all masses using two different boundary conditions (cutoff and IR).

4.4.1 Embedding

The slipping mode action is now given by

$$\tilde{\mathcal{S}}_{D7} = \int dr \sinh^4(r) \cos^3\theta(r) \sqrt{1 + \left(\frac{\partial\theta(r)}{\partial r}\right)^2}, \tag{4.23}$$

where the asymptotic boundary is located at $r \to \infty$, while the center of AdS is at $r = 0$. This results in the equation of motion

$$\begin{aligned}\left(\theta'(r)^2 + 1\right)\left(4\cosh(r)\theta'(r)\cos(\theta(r)) + 3\sinh(r)\sin(\theta(r))\right) \\ + \sinh(r)\theta''(r)\cos(\theta(r)) = 0.\end{aligned} \tag{4.24}$$

Here, it is still possible to embed the D7-brane using the cutoff boundary conditions

$$\begin{aligned}\theta(r_m) &= \frac{\pi}{2}, \\ \theta'(r_m) &= \Lambda,\end{aligned} \tag{4.25}$$

such that the brane depends on the radial coordinate and slips off of the pole at a finite value $r = r_m$. In addition to this, these coordinates allow for a second type of boundary condition

$$\begin{aligned}\theta(\epsilon) &= \alpha, \\ \theta'(\epsilon) &= \epsilon,\end{aligned} \tag{4.26}$$

where $0 \leq \alpha \leq 2\pi$, such that the position of the D7-brane is determined by dialing α.

4.4.2 Near-massless solutions

Extracting the analytic form of the linear fit of the smallest mass solutions proceeds by once again expanding the action in fluctuations $\theta(r)$ about the $r = 0$ boundary. Retaining only quadratic terms results in a linearized EOM in the IR. Then, solving the linearized EOM, allows one to analytically identify $c(m)$ in the near-massless regime. These solutions correspond to solving the EOM at a finite distance away from $r = 0$, as α will not be set to zero. The linearized EOM in this case is

$$-\sinh^4(r)\theta''(r) - 4\sinh^3(r)\cosh(r)\theta'(r) - 3\sinh^4(r)\theta(r) = 0, \tag{4.27}$$

and asymptotic solutions up to fourth order in the radial coordinate have the form

$$\theta(r) = \alpha_{(0)}e^{-r} + \alpha_{(1)}e^{-2r} + \alpha_{(2)}e^{-3r} + \beta_{(2)}re^{-3r}. \tag{4.28}$$

By inserting (4.28) into (4.27), switching to the z- coordinates with $r = -\log(z)$, then expanding about the asymptotic boundary $z = 0$ the coefficients were identified as $\alpha_{(1)} = 0$ and $\beta_{(2)} = 4\alpha_{(0)}$. Confirming that, in the r-coordinates, the solution has the expected form

$$\theta(r) = me^{-r} - 4mre^{-3r} + ce^{-3r}. \tag{4.29}$$

Then, by solving (4.10) with the IR boundary conditions (4.26) and the solution (4.29), the near-massless behavior of the condensate is identified as $c(m) = 3m$.

4.5 Numerics behind the horizon

For the medium to large masses the numerical differential equation solver NDsolve was used to iteratively solve the EOM (4.24) at different cutoffs r_m, using the cutoff boundary conditions (4.25), with $\epsilon = 10^{-3}$ and $\Lambda = 10^3$. This was implemented by a For-loop, containing NDsolve, which iterated through 20 different values of r_m. Each numerical solution was fit to a function of the form (4.29). The coefficients (m, c) were then collected from the fitting function and plotted. For the small mass limit, the boundary conditions were changed to (4.26) and iteration was instead performed for 20 values between $0 \leq \alpha \leq 2\pi$.

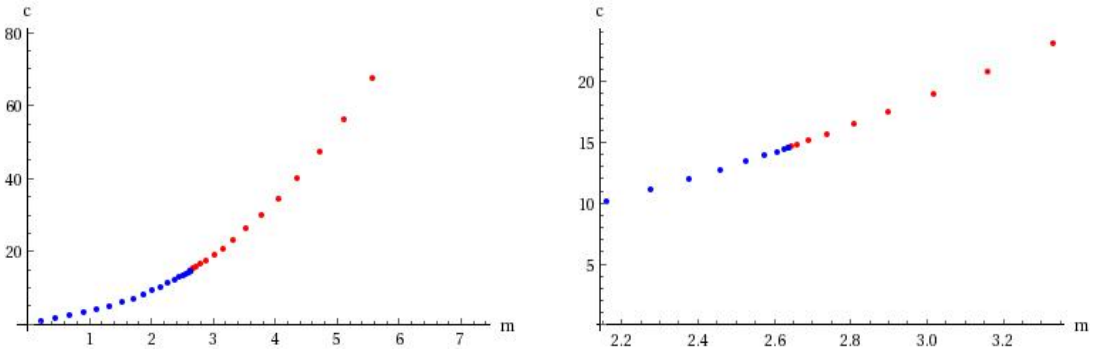

(a) **(b)**

Figure 4.5: (a) Small mass solutions acquired using α BC (4.26) (blue dots) versus medium mass solutions acquired using cutoff BC (4.25) (red dots). The red and blue dots meeting smoothly indicates a second-order phase transition between two different D7-branes at $m^* \approx 2.64$ and $c^* \approx 14.51$. As argued in [20], a smooth transition, in combination with a large vanishing cycle, suggests that the phase transition is second-order, as opposed to first-order which would be associated with a discontinuity. (b) Close-up view of phase transition in (a).

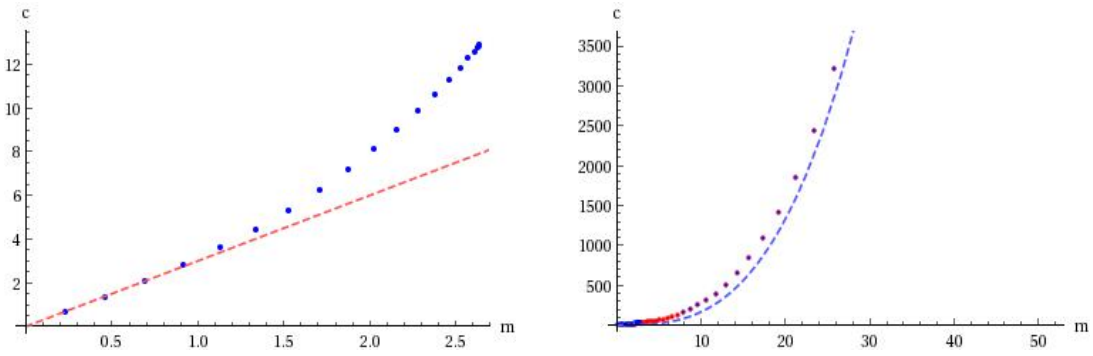

(a) **(b)**

Figure 4.6: (a) Smallest mass solutions acquired using α BC (4.26) (blue dots) can be seen converging toward the line $c(m) = 3m$ (b) Combined solutions including large masses acquired using cutoff BC (4.25) (purple dots). These solutions can be seen following the background solution $c(m) = m^3/6$.

5

Conclusion

In this thesis, the 1-point function of a strongly coupled hypermultiplet of flavor fields on dS_4, dual to the probe D7-brane slipping mode on dS_4-sliced AdS_5, was computed holographically. This was accomplished by first embedding the probe D7-brane in Minkowski foliated $AdS_5 \times S^5$. Following this, the first step of holographic renormalization was implemented at the level of the boundary conditions, ensuring regular solutions. This enabled a numerical confirmation of the known supersymmetric background solution. Then, the D7-brane was embedded in dS_4-sliced $AdS_5 \times S^5$, the asymptotic boundary solution was evaluated analytically, and the mass and condensate were computed numerically for both large and small masses. The numerical results suggested that at small masses $m \ll \frac{1}{\ell}$, the effects of de Sitter curvature to dominated the relationship between the mass and condensate parameters, where a linear relationship was found between m and c. At large masses $m \gg \frac{1}{\ell}$, the effects of de Sitter curvature become negligible in comparison to the effects of the mass, and the background solution reappeared $c = m^3/6$. In order to accurately describe the medium mass regime, in which neither the effects of de Sitter curvature or mass could be neglected, the subleading order mass correction was evaluated analytically to be $c = m^3/6 + \ell^{-2} m \log(m)/4$, and shown to fix the offset numerical solution. Thereafter, coordinates were switched in order to circumvent the de Sitter horizon, where the smallest mass solutions could be computed numerically. Moreover, this allowed a new type of D7-probe brane to be embedded in dS_4-sliced $AdS_5 \times S^5$, given by new boundary conditions. The near-massless solutions were evaluated analytically by solving equation of motion near the IR boundary, where the relationship was found to be $c = 3m$. The near-massless solutions were confirmed numerically for the new D7-brane embedding, and the largest mass solutions, acquired using the original D7-brane embedding, followed the background solution. A second-order phase transition was observed between the two D7-branes at the value $m^* \approx 2.64$ and $c^* \approx 14.51$.

The natural continuation of this investigation would be to use the acquired data to compute the strongly coupled 2-point correlation function dual to the slipping mode and to compare it to the weakly coupled 2-point function of slow-roll inflation. An initial aspect that requires further consideration is scale invariance. The 2-point function of slow-roll inflation is nearly scale invariant, while the 2-point function dual to the slipping mode has mass, violating scale invariance. Here, one could investigate the possibility of suppressing the breaking of scale invariance via the mass at strong coupling. If possible, a small violation of scale invariance should then yield a nearly scale invariant strongly coupled 2-point function.

Computationally, the holographic 2-point function would be acquired by solving the bulk equations of motion with small fluctuations added to the original solution $\theta(z) + \delta\theta(z, x, t)$. Here, an initial problem to tackle would concern time dependence. For Minkowski foliated AdS_5, it is possible to Fourier transform and replace the x and t dependence with k and ω. Computing the 2-point function on dS_4, on the other hand, requires commitment to a coordinate system. For global coordinates on dS_4, for example, x dependence could be replaced by spherical harmonics, but switching from time to frequency would complicate matters. Numerically computing 2-point function would correspond to solving linear partial differential equations of motion, where parameterizing solutions with frequency dependence could pose conceptual challenges.

Given the numerical computation of a strongly coupled 2-point function on dS_4, one could investigate the qualitative differences between observing a strongly and a weakly coupled inflaton. Here, however, one would have to take consideration to the fact that in the large N_c limit, correlation functions are suppressed by powers of N_c [5]. This entails that, although the holographic dual to scalar slipping mode is strongly coupled, the fact that it is also a large N_c theory may prevent any observable large non-Gaussianity.

Bibliography

[1] Daniel Baumann. Tasi lectures on inflation, 2009. arXiv:0907.5424 [hep-th].

[2] Eva Silverstein. Les houches lectures on inflationary observables and string theory, 2013. arXiv:1311.2312 [hep-th].

[3] Juan Maldacena. Non-gaussian features of primordial fluctuations in single field inflationary models. *JHEP*, 2003.

[4] Andreas Karch and Emanuel Katz. Adding flavor to ads/cft. *JHEP*, 2002.

[5] O. Aharony, S.S. Gubser, J. Maldacena, H. Ooguri, and Y. Oz. Large n field theories, string theory and gravity. *Phys.Rept.*, 1999. arXiv:hep-th/9905111.

[6] Donald Marolf, Mukund Rangamani, and Mark Van Raamsdonk. Holographic models of de sitter qfts. *Classical and Quantum Gravity*, 28(10), 2011.

[7] Kazuo Ghoroku, Masafumi Ishihara, and Akihiro Nakamura. Gauge theory in de sitter space-time from a holographic model. *Phys.Rev.D*, 2006.

[8] Adam B. Clark, Nathan Crossette, George M. Newman, and Andrea Rommal. Ads-sliced flavor branes and adding flavor to the janus solution. *Phys. Rev. D*, 2013.

[9] William H. Kinney. Tasi lectures on inflation, 2009. arXiv:0902.1529 [astro-ph.CO].

[10] J. Dunkley, E. Komatsu, M. R. Nolta, D. N. Spergel, D. Larson, G. Hinshaw, L. Page, C. L. Bennett, B. Gold, N. Jarosik, J. L. Weiland, M. Halpern, R. S. Hill, A. Kogut, M. Limon, S. S. Meyer, G. S. Tucker, E. Wollack, and E. L. Wright. Five-year wilkinson microwave anisotropy probe (wmap) observations: Likelihoods and parameters from the wmap data. *Astrophys.J.Suppl.*, 2008.

[11] Daniel Baumann and Liam McAllister. *Inflation and String Theory*. Cambridge University Press, 2015.

[12] J. Erdmenger M. Ammon. *Gauge/Gravity Duality Foundations and Applications*. Cambridge University Press, 2015.

[13] G. 't Hooft. A planar diagram theory for strong interactions. *Nuclear Physics*, 72, 1974.

[14] Daniel Z. Freedman Eric D'Hoker. Supersymmetric gauge theories and the ads/cft correspondence. TASI Lecture Notes, 2001. arXiv:hep-th/0201253.

[15] B. Zwiebach. *A First Course in String Theory*. Cambridge University Press, 2009.

[16] David Tong. Lectures on string theory, 2009. arXiv:0908.0333 [hep-th].

[17] Juan M. Maldacena. The large n limit of superconformal field theories and supergravity. *Adv.Theor.Math.Phys.*, 1997. arXiv:hep-th/9711200.

[18] Kostas Skenderis. Lecture notes on holographic renormalization, 2002. arXiv:hep-th/0209067.

[19] Marcus Spradlin, Andrew Strominger, and Anastasia Volovich. Les houches lectures on de sitter space, 2001. arXiv:hep-th/0110007.
[20] Andreas Karch, Andy O'Bannon, and Laurence G. Yaffe. Critical exponents from ads/cft with flavor. *JHEP*, 2009.
[21] C. Fefferman and C. Robin Graham. Conformal invariants. *Elie Cartan et les Mathematiques d'Aujourd'hui*, 1985.
[22] Willy Fischler, Sandipan Kundu, and Juan F. Pedraza. Entanglement and out-of-equilibrium dynamics in holographic models of de sitter qfts. *JHEP*, 2014.
[23] Mohsen Alishahiha, Andreas Karch, Eva Silverstein, and David Tong. The ds/ds correspondence. *AIP Conf.Proc.*, 2004. arXiv:hep-th/0407125.
[24] Andreas Karch, Andy O'Bannon, and Kostas Skenderis. Holographic renormalization of probe d-branes in ads/cft. *JHEP*, 2005.
[25] Andreas Karch and Andy O'Bannon. Chiral transition of n=4 super yang-mills with flavor on a 3-sphere. *Phys.Rev.D*, 2006.
[26] Jan Zaanen, Ya-Wen Sun, Yan Liu, and Koenraad Schalm. *Holographic Duality in Condensed Matter Physics*. Cambridge University Press, 2015.